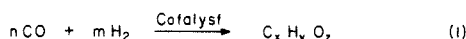


Bonding and Coupling of C<sub>1</sub> Fragments on Metal SurfacesChong Zheng,<sup>†,‡</sup> Yitzhak Apeloig,<sup>‡</sup> and Roald Hoffmann\*<sup>†</sup>

Contribution from the Departments of Chemistry and Materials Science Center, Cornell University, Ithaca, New York 14853, and Technion-Israel Institute of Technology, Haifa 32000, Israel. Received September 3, 1986

**Abstract:** The bonding of CH<sub>3</sub>, CH<sub>2</sub>, and CH fragments to Ti(0001), Cr(110), and Co(0001) metal surfaces is examined with extended Hückel band calculations on two-dimensional slabs of metal and adsorbate. A local chemical viewpoint is sought through fragment analyses, decompositions of the density of states, and overlap population studies. All fragments tend to restore their missing C-H bonds when bound to these surfaces—CH<sub>3</sub> prefers the on-top, CH<sub>2</sub> the bridging, and CH the capping geometry. CH<sub>3</sub> anchors more strongly to the on-top site of a metal surface of higher d band filling since the antibonding feature at the top of the d band destabilizes sites of higher coordination. Similar conclusions hold for other fragments. Thus, the mobility of these fragments is reduced on metal surfaces of higher d band filling. The mobility patterns of CH<sub>3</sub>, CH<sub>2</sub>, and CH are examined. In general, on the way to products there are barriers to migration on the surface, a proximity or crowding effect which makes it costly for two fragments to approach on the surface, a barrier, small or large, to the reaction with each other, and finally a desorption barrier. When two C<sub>1</sub> fragments couple, the C-C σ\* orbital rises from below the Fermi level. It is initially filled and then empties as the reaction proceeds. Hence the lower the Fermi level (for metals at the right side of the transition series) the smaller the reaction barrier. The theoretically expected decrease of the mobility of the organic fragments on one hand and the higher coupling rate on the other, as the metal is changed from the left to the right side in the Periodic Table, may be two of many reasons that are responsible for metals in the middle of the transition series having higher reactivity in Fischer-Tropsch catalysis.

The Fischer-Tropsch (FT) synthesis, which can be defined as the reductive oligomerization of carbon monoxide over a heterogeneous catalyst (eq 1), was described nearly 60 years ago.<sup>1,2</sup> Because of the great technological importance of this reaction much effort, especially during the last two decades, has been devoted to the elucidation of its mechanism.<sup>1-3</sup> Although the subject still continues to be strongly debated,<sup>4</sup> the accumulated



evidence suggests that under conditions that lead to oxygen-free products (i.e.,  $z = 0$  in eq 1) the FT reaction proceeds via the "carbide/methylene" mechanism,<sup>1-3</sup> which is drawn schematically in Scheme I. Under these conditions, the major products are α-olefins and hydrocarbons, and the oxygen ends up primarily as water, along with some oxygenated products.

The carbide/carbene mechanism was first suggested by Fischer and Tropsch themselves as early as 1926,<sup>2</sup> and it was re-introduced with additional details by Craxford and Rideal.<sup>3</sup> According to this mechanism carbon monoxide is first adsorbed and then dissociates on the metal surface to give "surface carbides" (step 1, Scheme I), which are then hydrogenated to give surface-bonded methylene and methyl fragments (step 2). The oligomerization of these metal-bonded fragments (step 3) is followed by a termination step such as a β-elimination (step 4), which followed by desorption yields the final products.<sup>1</sup>

The most extensive and convincing support for the carbide/methylene mechanism comes from the elegant studies by the research groups of Biloen<sup>5</sup> and Petit.<sup>6</sup> Biloen and Sachtler found that Ni-, Co-, and Ru-based catalysts, which are pre-doped with <sup>13</sup>C-labeled carbon, yield upon treatment with <sup>13</sup>CO/H<sub>2</sub> mixtures under FT conditions a product mixture consisting mainly of <sup>13</sup>CH<sub>4</sub> and of hydrocarbons containing several <sup>13</sup>C atoms in the same molecule.<sup>5</sup> These results indicate that the carbidic species, once formed, can react with hydrogen to give CH<sub>x</sub> intermediates ( $x = 1-3$ ), which polymerize to produce hydrocarbons, in agreement with steps 2 and 3 in Scheme I. The feasibility of the first step in the mechanism, in which the carbidic surface is formed, has been demonstrated convincingly by other investigators.<sup>7</sup> Thus, a rapid dissociative chemisorption of carbon monoxide has been shown to occur on various clean metal surfaces, including typical

FT catalysts such as iron.<sup>7</sup> More importantly, the formation of a "carbide layer" under real FT conditions is well-known.<sup>8</sup>

The beautiful studies of Petit and Brady on the induced decomposition of gaseous diazomethane (CH<sub>2</sub>N<sub>2</sub>) on typical FT catalysts provides additional strong and independent evidence for the operation of the carbide/carbene mechanism.<sup>6</sup> Decomposition of CH<sub>2</sub>N<sub>2</sub> on Ni, Pd, Fe, Co, Ru, and Cu surfaces, at atmospheric pressure and in the temperature range of 25–250 °C, produces only ethylene and dinitrogen.<sup>6</sup> This indicates that in the absence of hydrogen the adsorbed CH<sub>2</sub> fragments dimerize to ethylene (Scheme II), but polymerization to higher hydrocarbons does not occur. However, reaction of a mixture of H<sub>2</sub> and CH<sub>2</sub>N<sub>2</sub> over Co, Fe, and Ru surfaces, all typical FT catalysts, produces a variety of hydrocarbons with isomer and molecular weight distribution typical of a "real" FT reaction.<sup>6</sup> Furthermore, decomposition of CH<sub>2</sub>N<sub>2</sub> on surfaces that are not capable of dissociative chemisorption of H<sub>2</sub>, such as Cu, yields only ethylene, even in the presence of H<sub>2</sub>.<sup>6</sup> Wang and Ekerdt in a more recent study showed that pyridine can be used to scavenge C<sub>1</sub>–C<sub>3</sub> alkyl species from the surface of an iron catalyst during FT synthesis.<sup>9</sup> These findings are also consistent with the carbide/carbene mechanism in which alkyl fragments are the immediate precursors to the FT

(1) For recent reviews see: (a) Herrmann, W. A. *Angew. Chem., Int. Ed. Engl.* **1982**, *21*, 117. (b) Biloen, P.; Sachtler, W. M. H. *Adv. Catal.* **1981**, *30*, 165. (c) Keim, W., Ed. *Catalysis in C<sub>1</sub> Chemistry*; D. Reidel: Dordrecht, 1983. (d) Goodman, D. W. *Acc. Chem. Res.* **1984**, *17*, 194. (e) Anderson, R. B. *The Fischer-Tropsch Synthesis*; Academic: New York, 1984. (f) Anderson, J. R.; Boudart, M. *Catalysis*; Springer-Verlag: Berlin, 1981.

(2) Fischer, F.; Tropsch, H. *Brennst. Chem.* **1926**, *7*, 97; *Chem. Ber.* **1926**, *59*, 830.

(3) Craxford, S. R.; Rideal, E. K. *J. Chem. Soc.* **1939**, 1604.

(4) For a recent criticism of this mechanism see: Henri-Olivé, G.; Olivé, S. *J. Mol. Catal.* **1982**, *16*, 111. And for a counter-argument see: Smutek, M. *Ibid.* **1984**, *24*, 257.

(5) (a) Biloen, P.; Helle, J. N.; Sachtler, W. M. H. *J. Catal.* **1979**, *58*, 95; (b) Biloen, P. *Recl. Trav. Chim. Pays-Bas* **1980**, *99*, 33.

(6) Brady, R. C., III; Petit, R. *J. Am. Chem. Soc.* **1980**, *102*, 6181; **1981**, *103*, 287. For more recent related studies see: Bock, H.; Tschmutova, G.; Wolf, H. P. *J. Chem. Soc., Chem. Commun.* **1986**, 1068.

(7) (a) Low, G. G.; Bell, A. T. *J. Catal.* **1979**, *57*, 397. (b) Joyner, R. W.; Roberts, M. W. *Chem. Phys. Lett.* **1974**, *29*, 447. (c) Roberts, M. W. *Chem. Soc. Rev.* **1977**, *6*, 373. (d) Brodén, G.; Rhodin, T. N.; Brucker, C.; Benbow, R.; Hurych, Z. *Surf. Sci.* **1976**, *59*, 593.

(8) Frohning, C. D.; Kölbl, H.; Ralek, M.; Rottig, W.; Schnur, F.; Schulz, H. In *Chemierohstoffe aus Kohle*; Balbe, J., Ed.; Thieme: Stuttgart, 1977; Chapter 8, pp 219–299.

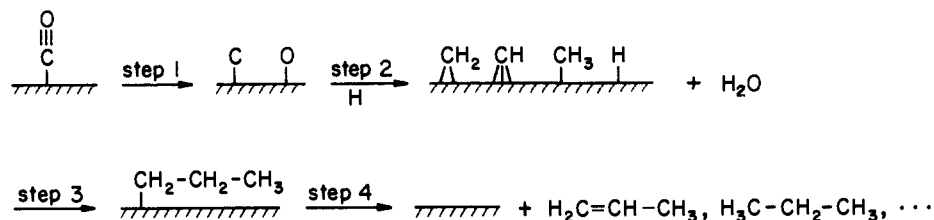
(9) Wang, C. J.; Ekerdt, J. G. *J. Catal.* **1984**, *86*, 239.

<sup>†</sup> Present address: Department of Chemistry, University of Houston, Houston, TX 77004.

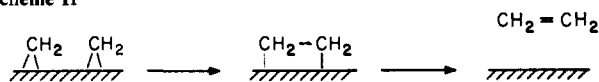
<sup>‡</sup> Cornell University.

<sup>‡</sup> Technion-Israel Institute of Technology.

Scheme I



Scheme II



products. In another important recent paper, Ekstrom and Lapszewicz showed that high molecular weight hydrocarbons can be formed by the reaction of carbides with hydrogen in the presence of water.<sup>10</sup> Furthermore, Winograd et al. have recently reported the detection of CH, CH<sub>2</sub>, and CH<sub>3</sub> intermediates on a Ni(111) methanation catalyst,<sup>11a</sup> and Ceyer and co-workers have observed CH<sub>3</sub> on a Ni(111) surface.<sup>11b</sup> Also Copperthwaite and co-workers presented X-ray photoelectron spectroscopic evidence for C-C bond formation during the interaction of chemisorbed CO with diazomethane on a polycrystalline iron surface.<sup>11c</sup>

Additional support, although indirect, for the chemical feasibility of the various steps of the carbide/methylene mechanism stems from the study of appropriate model organometallic complexes. Substantial experimental effort has been devoted in the last decade to the study of such model complexes.<sup>1a</sup> Relevant systems and molecular reactions will be mentioned briefly throughout the paper, and reviews (in addition to ref 1a) are gathered in ref 12. We note that metal-bound fragments such as methylene and methyl might be important intermediates also in other reactions occurring on metal surfaces, such as olefin metathesis and alkane activation processes.

Despite the extensive study of the FT synthesis many of the mechanistic details remain poorly understood. In particular, there is virtually no knowledge of the electronic and geometrical factors that control the polymerization process (step 3, Scheme I), and very little is known of the nature of the bonding of the organic fragments to the surface. Representative questions that remain unanswered are the following: What are the most effective binding sites on the metal surface for the adsorbed fragments and are these sites the same for all radicals? What is the favored orientation for the coupling of two methylenes to produce ethylene (Scheme II)? Are the binding sites and the dimerization mechanism the same for different metals? What is the relative mobility of CH<sub>2</sub> and CH<sub>3</sub> fragments on the metal surface, and how does this mobility change as the metal is varied? At present these and similar questions are difficult to answer experimentally, although encouraging advances have been made recently.<sup>13</sup> We will address these and other interesting mechanistic questions regarding the FT synthesis in this paper.

A full theoretical treatment of the FT reaction is a vast project, and we have to impose some limitations on the scope of problems

that will be tackled. In this study we concentrate on three major issues: (1) the mode of binding of the postulated reaction intermediates—methyl, methylene, and methyne—to the metal surface; (2) the mobility of these radicals on the metal surface; and (3) the electronic and geometrical requirements for the surface-induced coupling of the organic radicals.

We use in our work tight binding extended Hückel calculations,<sup>14</sup> with details given in Appendix I. The analysis of the surface calculations is based on the methodology and the tools that we have described in detail in our recent study of C-H and H-H activation on surfaces.<sup>15</sup> The extended Hückel method, whether applied to discrete molecules or extended systems, has well-known limitations. It does not do well at predicting distances, and this will impose severe limitations in the analyses of mobility and coupling. But the method does seem to capture the essence of bonding. It is also transparent and useful in constructing explanations, and it is for this reason that we use it.

While many of the problems we will attack have not been investigated theoretically before, some have. The relevant studies of Baetzold, Muetterties, and Shustorovich,<sup>16,17</sup> of Minot, Van Hove, and Somorjai,<sup>18a</sup> and of Anderson<sup>18b-d</sup> as well as other related theoretical work<sup>18c</sup> will be discussed in this paper. We also note that the first step of the FT reaction, the chemisorption of CO on various metal surfaces, has been studied extensively by many theoreticians.<sup>17,18b-d,19</sup>

This will be a long paper. It could easily have been chopped up into three papers, one on fragment bonding, a second on migration, a third on fragment coupling. We think nothing would be gained by this, and continuity would be lost. We ask the reader to bear with us as we analyze, in detail, an important reaction at the border of chemistry, physics, and catalysis.

## General Considerations

The FT synthesis occurs on Fe and Co catalysts and to some extent also on Ni surfaces.<sup>1</sup> A major goal of any mechanistic study of the FT synthesis is to try to define and understand the factors that determine the catalytic reactivity of the metal surface. In this respect two key parameters are the identity of the metal and the lattice form in which it crystallizes.<sup>13,20</sup> For each metal, one

(10) Ekstrom, A.; Lapszewicz, J. *J. Phys. Chem.* **1984**, *88*, 4577.

(11) (a) Kaminsky, M. P.; Winograd, N.; Geoffroy, G. L.; Vannice, M. A. *J. Am. Chem. Soc.* **1986**, *108*, 1315. For other related studies see references therein. (b) Lee, M. B.; Yang, Q. Y.; Tang, S. L.; Ceyer, S. T. *J. Chem. Phys.* **1986**, *85*, 1693. (c) Ceyer, S. T.; Beckerle, J. D.; Lee, M. B.; Tang, S. L.; Yang, Q. Y.; Hines, M. A. *J. Vac. Sci. Technol.*, in press. (d) Loggenberg, P. M.; Carlton, L.; Copperthwaite, R. G.; Hutchings, G. J. *J. Chem. Soc., Chem. Commun.* **1987**, 541.

(12) (a) Hahn, J. E. *Prog. Inorg. Chem.* **1984**, *31*, 205. (b) Holton, J.; Lappert, M. F.; Pearce, R.; Yarrow, P. I. W. *Chem. Rev.* **1983**, *83*, 135. (c) Nutton, A.; de Miguel, A. V.; Isobe, K.; Maitlis, P. *J. Chem. Soc., Chem. Commun.* **1983**, 166. (d) Saez, I. M.; Meanwell, N. J.; Nutton, A.; Isobe, K.; Vázquez de Miguel, A.; Bruce, D. W.; Okeya, S.; Andrews, D. G.; Ashton, P. R.; Johnstone, I. R.; Maitlis, P. M. *J. Chem. Soc., Dalton Trans.* **1986**, 1565.

(13) (a) For an excellent review see: Somorjai, G. A. *Chem. Soc. Rev.* **1984**, *13*, 321. (b) Koestner, R. J.; Van Hove, M. A.; Somorjai, G. A. *J. Phys. Chem.* **1983**, *87*, 203.

(14) (a) Hoffmann, R. *J. Chem. Phys.* **1963**, *39*, 1397. (b) Hoffmann, R.; Lipscomb, W. N. *Ibid.* **1962**, *36*, 2179. (c) For the implementation of the E.H. formalism to generate band structures, see: Whangbo, M.-H.; Hoffmann, R.; Woodward, R. B. *Proc. R. Soc. (London)* **1979**, *A-366*, 23.

(15) Saillard, J.-Y.; Hoffmann, R. *J. Am. Chem. Soc.* **1984**, *106*, 2006.

(16) Shustorovich, E.; Baetzold, R. C.; Muetterties, E. L. *J. Phys. Chem.* **1983**, *87*, 1100.

(17) (a) Baetzold, R. C. *J. Phys. Chem.* **1984**, *88*, 5583. (b) Baetzold, R. C.; Monnier, J. R. *J. Phys. Chem.*, accepted for publication.

(18) (a) Minot, C.; Van Hove, M. A.; Somorjai, G. A. *Surf. Sci.* **1982**, *127*, 441. (b) Anderson, A. B.; Onwood, D. D. *Surf. Sci.* **1985**, *154*, L261. (c) Ray, N. K.; Anderson, A. B. *Surf. Sci.* **1983**, *125*, 803; *119*, 35. (d) Anderson, A. B. *Surf. Sci.* **1977**, *62*, 119. (e) Vetrivel, R.; Viswanathan, B. *J. Mol. Catal.* **1984**, *24*, 245.

(19) (a) Sung, S.-S.; Hoffmann, R. *J. Am. Chem. Soc.* **1985**, *107*, 578. (b) Blyholder, G. *J. Phys. Chem.* **1964**, *68*, 2772. (c) Anderson, A. B. *J. Chem. Phys.* **1976**, *64*, 4046. (d) van Santen, R. A. *Proc. Int. Congr. Catal.*, *8th*, **1984**. (e) Andreoni, W.; Varma, C. M. *Phys. Rev. B* **1981**, *23*, 437. (f) Allison, J. N.; Goddard, W. A., III. *Surf. Sci.* **1981**, *110*, L615. (g) Doyen, G.; Ertl, G. *Surf. Sci.* **1977**, *B5*, 641; *69*, 157. (h) Bagus, P. S.; Hermann, K. *Phys. Rev. B* **1977**, *16*, 4195. (i) Davenport, J. W. *Phys. Rev. Lett.* **1976**, *36*, 945. (j) Bullett, D. W.; Cohen, M. L. *J. Phys.* **1977**, *C10*, 2101. (k) Andzelm, J.; Salahub, D. R. *Int. J. Quantum Chem.* **1986**, *29*, 1091.

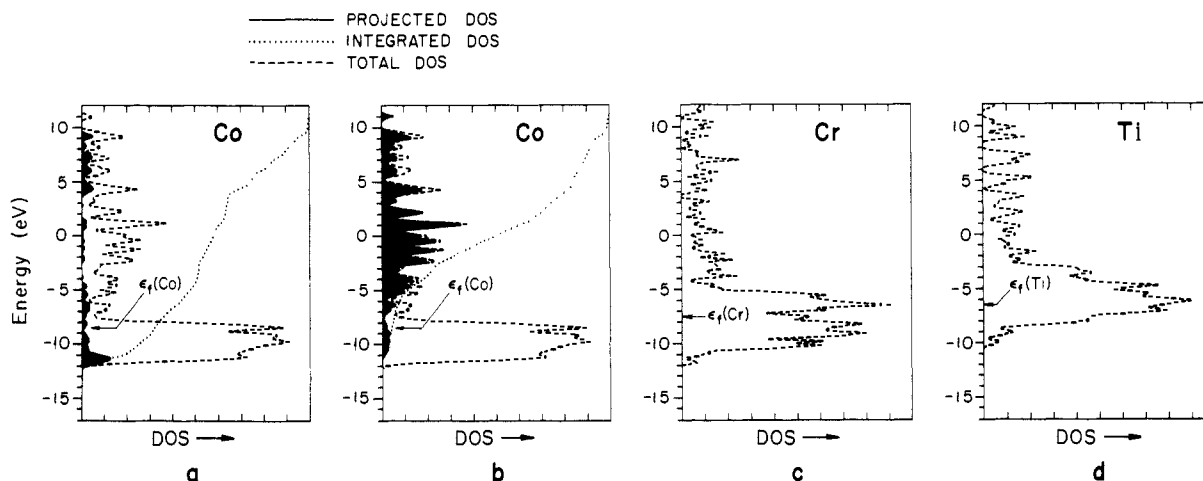
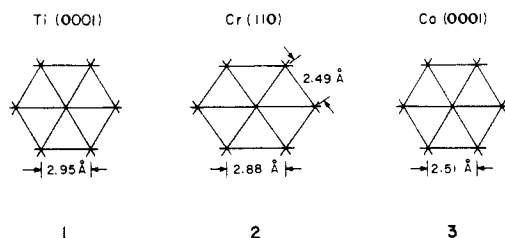


**Figure 1.** Total DOS (dashed lines) of the Co(0001), Cr(110), and Ti(0001) three-layer slabs. The darkened areas show the contribution from s and p states in parts a and b, respectively, for the Co case.  $\epsilon_f$  indicates the Fermi level. Cr and Ti total state densities are shown in parts c and d. The d band center of gravity and the Fermi level shifts to higher energy on going from Co to Ti.

can choose surfaces with different indices, and generally each surface is expected to exhibit a different reactivity. We are going to use a fixed surface throughout the paper, to model what must be only one aspect of reality. The surface we chose is the (0001) surface of a hexagonal metal. With the high symmetry of this surface the computational times can be greatly reduced. For example, when a methyl group is adsorbed on this surface in an "on-top" or "threefold" geometry, the hexagonal symmetry is still retained and the computational advantage of this over other surfaces of FT catalysts (e.g., Fe(110)) is obvious. The results can also be compared with our previous studies on other hexagonal surfaces.<sup>15,21</sup>

To extract the basic electronic effects that determine the reactivity of the metal, we are going to compare three metal surfaces: Ti(0001), Cr(110), and Co(0001). They are shown in 1, 2, and 3, respectively. Although the Cr(110) surface is not hexagonal, it can be viewed as a distortion therefrom.



Let us begin with the hcp lattice of cobalt and employ the experimental Co-Co distance of 2.51 Å. The next choice to be made is that of the thickness of the slab of the metal to be used in the calculations, of necessity a compromise between computational economy and reasonable accuracy. Our previous studies<sup>14c,15,19a,21</sup> as well as exploratory calculations on the cobalt slab lead to the conclusion that a reasonable choice is a 3-layer slab. We use here a slab of three layers because the changes in the important surface properties (e.g., the Fermi level, charge distribution, overlap population, etc.) are small on going to a 4-layer slab. The 3-layer slab model for the hcp Co surface is shown in a side view in 4. We choose the z axis to be perpendicular to the

surface. A top view is in 5, where the dots in the triangular hollows represent the Co atoms in the next layer below.

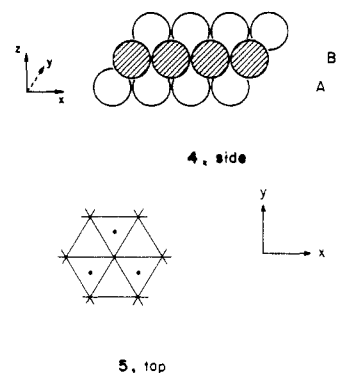


Figure 1 shows the density of states (DOS) curve of the slab. A DOS curve is the solid-state analogue of an energy level diagram and it gives the number of levels in a particular energy interval. The metal bands (or orbitals) are filled up to the Fermi level—the solid-state equivalent of the molecular HOMO. The dashed lines in Figure 1 refer to the total DOS curve. The darkened areas indicate the contribution of the s (Figure 1a) and the p states (Figure 1b) to the total DOS. The darkened areas are examples of projected or local DOS curves that single out the contribution of a certain atom or a group of atomic or fragment orbitals to the overall DOS plot. The states that are not s or p are d states. The dotted lines are integration curves, from 0 to 100%, which additionally count the relative number of states occupied as one sweeps up the energy scale. It is clear from Figure 1 that a substantial number of s and some p states penetrate into the d band. On the average any Co atom has its s band approximately one-third filled.

In any reactivity problem, molecular or solid state, the energy and bonding capabilities of the frontier orbitals, the lower unoccupied and higher occupied orbitals of the system will play a crucial role. In the case of a metal surface these are the orbitals near the Fermi level. It is important to know how the essential features of these frontier orbitals of the surface change as the metal is varied. As the number of d electrons increases from Ti to Co, the nuclear charge is less effectively "screened" and d electrons are more strongly bound by the bigger Coulomb interaction. There are therefore two factors competing in the determination of the Fermi level: the filling of the d band, which tends to raise the Fermi level, and the Coulomb interaction that pulls down the Fermi level with increasing d electron count. It turns out that the Coulomb interaction wins out, and the Fermi level descends slowly along the right side of the transition series (the relevant work functions are Ti 4.33, Cr 4.5, Co 5.0 eV<sup>20d</sup>). Another

(20) (a) Ashcroft, N. W.; Mermin, N. D. *Solid State Physics*; Saunders College: Philadelphia, 1976. (b) Kittel, C. *Introduction to Solid State Physics*; J. Wiley: New York, 1976. (c) Harrison, W. A. *Solid State Theory*; Dover Publications Inc.: New York, 1980. (d) Shustorovich, E.; Baetzold, R. C.; Muettterties, E. L. *J. Phys. Chem.* **1983**, *87*, 1100. Baetzold, R. C. *Solid State Commun.* **1982**, *44*, 781. Varma, C. M.; Wilson, A. J. *Phys. Rev. B* **1980**, *22*, 3795. Varma, C. M. *Ibid.* **1981**, *23*, 437. The difference in work function between Mn and Cu is  $\sim 1$  eV, see: *Handbook of Thermionic Properties*; Samsanov, G. V., Ed.; Plenum Press Data Division: New York, 1966. Michaelson, H. B. *J. Appl. Phys.* **1977**, *48*, 4729.

(21) (a) Silvestre, J.; Hoffmann, R. *Langmuir* **1985**, *1*, 621. (b) Silvestre, J.; Hoffmann, R. *Helv. Chim. Acta* **1985**, *68*, 1461.

**Table I.** Electron Distribution among the Metal Atomic Orbitals of Co(0001), Cr(110), and Ti(0001) Slabs (Coordinate Axes Are Given in 4)

orbital	Co d <sup>9</sup>		Cr d <sup>6</sup>		Ti d <sup>4</sup>	
	"surface"	"bulk"	"surface"	"bulk"	"surface"	"bulk"
d <sub>x<sup>2</sup>-y<sup>2</sup></sub> or d <sub>xy</sub>	1.57	1.54	1.03	0.90	0.63	0.57
d <sub>z<sup>2</sup></sub>	1.73	1.51	1.04	0.95	0.57	0.57
d <sub>xz</sub> or d <sub>yz</sub>	1.76	1.45	1.05	0.86	0.59	0.61
s	0.65	0.62	0.75	0.67	0.80	0.73
p	0.26	0.29	0.33	0.31	0.22	0.30
total	9.31	8.39	6.29	5.42	4.02	3.95

consequence of the increasing Coulomb attraction is the decreasing d band width along the transition series, due to the "tighter" wave functions of the d electrons. The calculations confirm these general considerations. The extended Hückel method, as usual, gives a much too high magnitude of the ionization potential or Fermi level. It does so for molecule as well as for extended structures.

In analogy to our previous studies<sup>15,21</sup> we find that the charge distribution among the slab layers changes as a function of the number of electrons per metal atom. Basically, this results from the fact that an inner atom has more neighbors than a surface one. The band dispersion is a function of inter-unit-cell interaction, so that the more interactions (neighbors) one has, the wider the resulting band is. Thus the states of the "surface atoms" (layer A in 4) form narrower bands than the bulklike atoms (layer B in 4). The wider bulk bands are filled first and thus the bulk atoms become negative relative to the surface. At some point along the transition series the two layers will have equal charges, and past this point the surface layer will become negative. The conclusion from these qualitative arguments is that at the right side of the transition series surfaces are expected to be negative relative to the bulk (or to the isolated atom), while at the left side of the transition series surfaces are expected to be positive.

The calculations fully support these conclusions. For Co we find that each of the surface atoms carries a negative charge of 0.31 electron (note that because of the ABA arrangement the charge on each bulk metal is twice as large and of opposite sign to charge on a surface atom). For Cr we get a negative charge of -0.29 at a surface atom. For Ti the polarization is small and both surface and bulk layers are nearly neutral (each surface Ti atom carries a charge of 0.03 electron). To put these charge distributions in a chemical context we might say that the surface layers of the Co and Cr slabs can be described as being nucleophilic and Ti neutral. Better calculations will temper the indubitably exaggerated density shifts between surface and bulk, but the trend should remain.

Another important difference between the surface and the bulk atoms, shown in Table I, is in the electron distribution between the atomic metal orbitals. Let us examine first the surface. The data in Table I reveal in the Co case a significant electron flow from the "in-plane" orbitals (d<sub>x<sup>2</sup>-y<sup>2</sup></sub>, d<sub>xy</sub>) into orbitals that are perpendicular to the surface (d<sub>z<sup>2</sup></sub>, d<sub>xz</sub>, d<sub>yz</sub>). But as the d electron filling decreases the situation is reversed: for Ti there is an electron flow from d<sub>z<sup>2</sup></sub>, d<sub>xz</sub>, and d<sub>yz</sub> to d<sub>x<sup>2</sup>-y<sup>2</sup></sub> and d<sub>xy</sub>. This is again due to the fact the "in-plane" orbitals on the surface overlap better with their neighbors, resulting in a wider band. At low electron counts these orbitals are filled first, but as the filling increases the narrower bands, which are at intermediate energy, are filled more.

For the bulk orbitals, the perpendicular orbitals (d<sub>z<sup>2</sup></sub>, d<sub>xz</sub>, d<sub>yz</sub>) overlap not only with orbitals in the same plane (B in 4) but also with the layers sandwiching them (A layers in 4), thus the band widths are bigger than those of d<sub>x<sup>2</sup>-y<sup>2</sup></sub> and d<sub>xy</sub>. For the same reason that we have adduced above the charge flows from d<sub>z<sup>2</sup></sub>, d<sub>xz</sub>, and d<sub>yz</sub> to d<sub>x<sup>2</sup>-y<sup>2</sup></sub> and d<sub>xy</sub> at high electron counts, but it is reversed for low electron fillings.

We are now in a position to bring to the surface a layer of organic molecules.

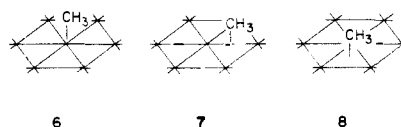
#### General Considerations for Adsorption of Methyl, Methylene, and Methyne Radicals on Metal Surfaces

In order to study the adsorption of CH<sub>x</sub> (x = 1-3) radicals on the metal surface we have to simplify the calculations further by

covering only one side of the 3-layer slab. For justification we rely on our previous study which showed that very similar results are obtained for a coverage of a 4-layer Ni slab with H<sub>2</sub> on one side or on both sides.<sup>15</sup> Please see Appendix II for further discussion.

The one-side coverage makes the two identical A layers in 4 different in the covered metal slab. The top layer A can be described as the "adsorbing" layer, the inner layer B is the "bulklike" layer, and the bottom layer is similar in character to the surface layer A in the bare metal (except for a small perturbation by the remote adsorbent).

We have studied the adsorption of three organic radicals, CH<sub>3</sub>, CH<sub>2</sub>, and CH, all believed to be intermediates in the FT synthesis.<sup>1</sup> Regardless of the geometry that is chosen, a 1:1 coverage of the metal surface by CH<sub>3</sub> or CH<sub>2</sub> is chemically unrealistic due to the very short distances and the resulting excessive steric repulsions between the hydrocarbons. We have chosen a one-third coverage, which ensures minimal interactions between neighboring fragments but which still allows the use in the calculation of a convenient unit cell that is only three times larger than that in the bare metal. The details concerning the unit cell that was used, the Brillouin zone, the special *k* points, etc., are given in Appendix I. For each of the organic radicals we have considered three possible adsorption sites: a mono-coordinated "on-top" site 6, a site "bridging" two metal atoms 7, and a "triply bridging", "capping", or "hollow" site 8.



As in our previous studies<sup>15,19,21</sup> we use the language and formalism of simple perturbation theory. Within this framework the interaction of two levels,  $\Delta E$ , is given by eq 2. The magnitude of the matrix element  $H_{ij}$  in the numerator is related to the overlap

$$\Delta E = \frac{|H_{ij}|^2}{E_i^0 - E_j^0} \quad (2)$$

of the relevant orbitals, and the denominator tells us that the interaction is greater the closer in energy the two orbitals are, i.e., the more the two orbitals come into resonance.

The consequence of orbital interactions between the metal bands and the orbitals of the organic fragment can be traced down and analyzed by examining the DOS curves. Contributions or projections of specific orbitals are particularly helpful. In general, a strong shift in the position of a particular fragment orbital as it approaches the metal surface indicates strong interaction, either bonding or antibonding. A small shift, on the other hand, indicates little interaction.

Another important tool for the analysis is the COOP (for Crystal Orbital Overlap Population) curve, which gives the relative number of levels in a given energy interval weighted by the contribution that these levels make to the overlap population of a specified bond. In other words a COOP curve allows us to determine if a collection of energy levels contributes to bonding or antibonding between two atoms or fragments. We find that both the DOS and the COOP curves, but in particular their combination, are very effective in analyzing the bonding properties of metal surfaces.<sup>14c,15,19,21</sup> The use of these tools will be dem-

**Table II.** Methyl-Surface Interactions (see 10) and Their Expected Consequences

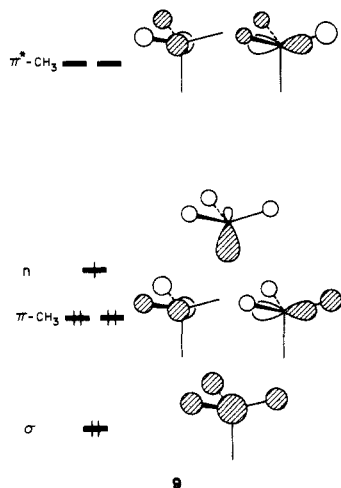
interaction	no. of electrons	stabilizing?	effective?	charge transfer
①	1	yes	yes	to M
①	3	yes	yes	to CH <sub>3</sub>
②	0	no	no	none
②	2	yes	no	to CH <sub>3</sub>
③	2	yes	no	to M
③	4	no	no	none

onstrated throughout the paper.

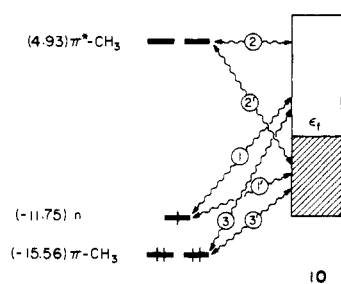
We proceed now to analyze in some detail the bonding between each of the organic radicals and the metal surface.

### Adsorbed Methyl

The orbitals of the methyl fragment are well-known and they are shown in 9. We arbitrarily choose to define the methyl fragment as a radical so that at infinite separation both the metal and the radical are neutral. The HOMO of the methyl radical



is n-CH<sub>3</sub>, a nonbonding type orbital at -11.75 eV. This orbital, which we will call n, is singly occupied. Lower in energy, at -15.56 eV, are the two degenerate π-CH<sub>3</sub> orbitals and still lower is the σ-CH<sub>3</sub> orbital. The LUMO consists of the two degenerate π\*-CH<sub>3</sub> orbitals at 4.93 eV.



There are many interaction modes between the methyl radical and the metal slab, but the perturbation expression helps one sort these out. In the schematic diagram 10 we have assigned numbers ①, ②, and ③ to the interactions of n, π\*-CH<sub>3</sub> and π-CH<sub>3</sub> with the unfilled band states of the surface slab and ④, ②, and ③ to the interaction with filled metal states. Whether these are overall stabilizing or destabilizing is a function of the orbital filling. The magnitude of the interactions obviously depends critically on both the separation in energy between the interacting orbitals and the effectiveness of the overlap in question. Table II contains a qualitative summary of our expectations, including the anticipated direction of charge transfer that is a consequence of each interaction in 10.

A word of explanation is needed on these expectations. Normally the focus would be on two-electron bonding interactions,

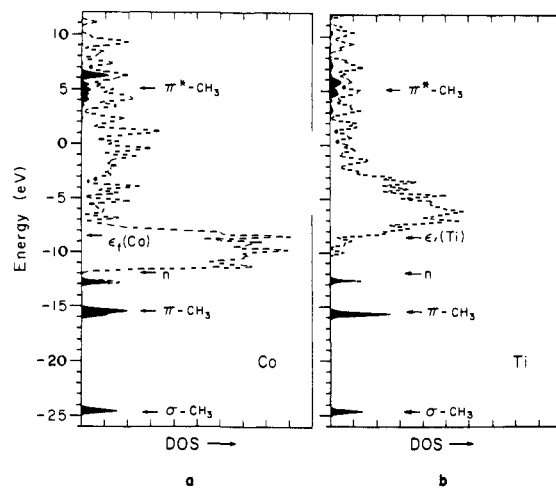


**Figure 2.** Total DOS (dashed line) and the CH<sub>3</sub> contribution (darkened area) when a CH<sub>3</sub> group is chemisorbed in an on-top geometry on Co(0001) (a) and Ti(0001) (b) surfaces. The arrows indicate the CH<sub>3</sub> MO levels before the adsorption occurs.

for these are both stabilizing and effective in charge transfer. But in the case at hand none of the interactions of this type, ② or ③, is very good, because the orbitals in question are far from resonance. Instead interactions ① and ④ of the methyl radical orbital become most important. And interaction ①, typical of energetically ambiguous and difficult to analyze 3-electron interactions, will be crucial.

In addition to these interactions, all of which have molecular equivalents, we have interaction ④, characteristic of surfaces. Interaction ④ represents schematically the metal slab's ability to shift electron density between the bulk and surface layers, or on the surface to shift density between those metal atoms involved in bonding and those left alone. This occurs in response to the electronic demands imposed by interactions with the organic adsorbate.

We can trace the validity of the perturbation theory based characterization of the primary interactions by examining the consequences or symptoms of interaction in the DOS curves in Figure 2a. This is for methyl on Co(0001) in the on-top geometry. Projections of the methyl orbitals are darkened and the position of these orbitals in the isolated organic fragments are indicated by arrows.

As expected, the σ-CH<sub>3</sub> and the π-CH<sub>3</sub> bands of the adsorbed CH<sub>3</sub> are essentially at the same energy as in the isolated radical and their bands are narrow—a clear indication of their weak interaction with the surface. In contrast, the energies of the n and the π\*-CH<sub>3</sub> orbitals change significantly upon interaction with the metal. The n band is pulled down to a lower energy (by ~1 eV), while the π\*-CH<sub>3</sub> band is pushed up in energy approximately to the same degree. The large shifts of these orbitals relative to the orbitals of the isolated radical are clear indications of their strong interaction with the surface. The interaction, of course, depends on the M-C distance. The DOS in Figure 2 are calculated for a typical M-C distance of 2.1 Å (for the choice of the M-C distance see Appendix I).

Figure 2b is the DOS curve for the Ti case. Since the center of gravity of the d band and the Fermi level are higher in energy, we should expect a weaker interaction between the metal and the CH<sub>3</sub>. n in Figure 2b is pushed down less than in Figure 2a. However, the main feature remains the same. The Cr case is intermediate between the Co and Ti, and we omit it.

### CH<sub>3</sub> in the On-Top Geometry

We will analyze this specific case in more detail than the others so as to demonstrate how the DOS and COOP curves may be used to understand the bonding. The other geometries can be then analyzed in less detail. We concentrate on the Co surface. The DOS curve of geometry 6 (Figure 2) was already discussed above. We have concluded that among the methyl orbitals only the n and

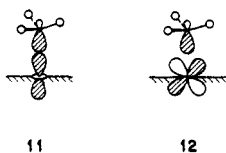
**Table III.** Some Details of Energetics and Electron Distribution for Three Sites of Methyl Binding to Co(0001), Cr(110), and Ti(0001) Surfaces

		Fermi level (eV)	binding energy (eV)		overlap population						
			$E_1$	$E_2$	$M_1-M_2$	$M_1-C$	$M_2-C$	$M_1-H_1$	$M_2-H_1$	C-H <sub>1</sub>	C-H <sub>2</sub>
	Ti	-6.48			0.35						
	Cr	-7.50			0.46						
	Co	-8.48			0.18						
	Ti	-6.47	5.42	0.16	0.29	0.37		-0.04	-0.00	0.81	0.81
	Cr	-7.51	4.29	0.09	0.41	0.42		-0.04	-0.01	0.80	0.80
	Co	-8.48	3.73	0.47	0.17	0.42		-0.02	-0.00	0.79	0.79
	Ti	-6.43	4.89	-0.36	0.16	0.18	0.20		0.01	0.79	0.79
	Cr	-7.40	3.36	-0.84	0.26	0.23	0.21		0.01	0.77	0.77
	Co	-8.47	2.64	-0.62	0.11	0.22	0.21		-0.00	0.78	0.80
	Ti	-6.48	5.3	0.06	0.19	0.17	0.17	0.10		0.74	0.74
	Cr	-7.34	3.36	-0.85	0.28	0.17	0.16	0.06		0.76	0.76
	Co	-8.45	2.36	-0.90	0.11	0.17	0.17	0.01		0.77	0.77

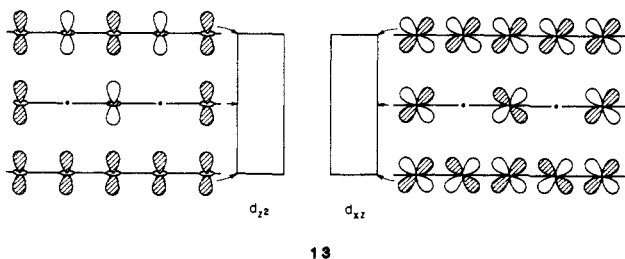
<sup>a</sup>  $E_1 = [E(\text{slab}) + E(\text{CH}_3)] - E_{\text{total}}$ ;  $E_2 = [E(\text{slab}^+) + E(\text{CH}_3^-)] - E_{\text{total}}$ . Thus the positive signs mean CH<sub>3</sub> or CH<sub>3</sub><sup>-</sup> is bound.  $E_2$  measures the covalent contribution to the total binding energy  $E_1$ .

$\pi^*$ -CH<sub>3</sub> orbitals contribute to metal-carbon bonding (i.e., interactions ①, ①, and ② in 10). We proceed now to examine these interactions in more detail.

We shall begin with interaction between the n-CH<sub>3</sub> orbital and the metal bands. If we were in a discrete mono-nuclear complex then we could simply say that the  $\sigma$  nature of the CH<sub>3</sub> n orbital allows interaction with  $d_{z^2}$ , 11, but prohibits them with, say  $d_{xz}$ , 12. Life is not so simple in the solid. Each metal orbital spreads out into a band. Local interactions are dominant, but symmetry limitations on interaction are not so strong. We often have to replace statements such as "does (or does not) interact with a given level" by "interacts more (or less) with such and such part of a band".

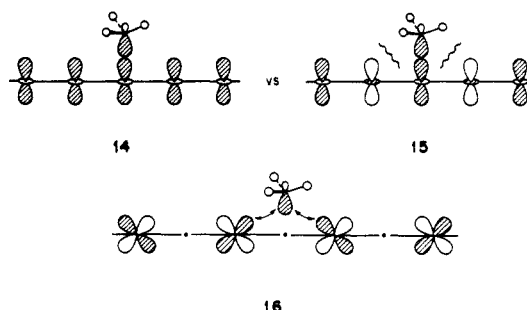


Let us illustrate this point qualitatively with the interaction of n. In the metal there is not one  $d_{z^2}$  and  $d_{xz}$  orbital but many. 13 illustrates schematically some representative orbitals in the  $d_{z^2}$  and  $d_{xz}$  bands. The orbitals at the bottom of a band are metal-metal bonding, those in the middle nonbonding, and those at the top antibonding. Things are more complicated in three (or two) dimensions, but these one-dimensional representations are indicative of what transpires.



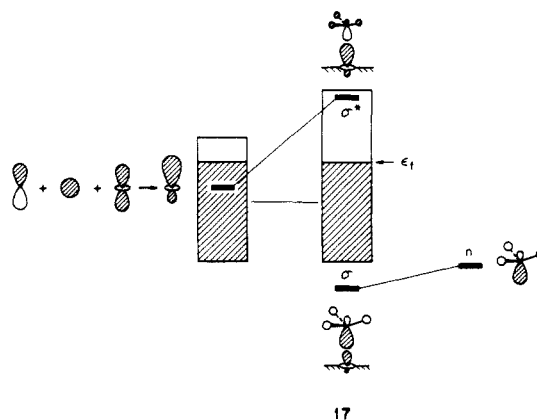
What we can say now is that n interacts with the entire  $d_{z^2}$  band, but perhaps more strongly with the bottom of the band than with the top, judging by the overlap differences between 14 and 15. For interaction with the  $d_{xz}$  band, the overlap is strictly zero only at the zone center and edge (the most antibonding and bonding combinations, respectively). It is never very efficient, but as 16 shows, one can have an overlap between the middle of the  $d_{xz}$  band and n. Still, the overlap in 16, depending as it does on non-nearest-neighbor interaction, is not very good for on-top adsorption. So in analogy to discrete complexes we can focus our attention on locally strong  $\sigma$  interactions. In addition to  $d_{z^2}$ , s and  $p_z$  have the proper local symmetry to interact. They will do so, but the

mixing with  $p_z$  is not great since it is very high in energy relative to n.



The interactions between n of substrate and the surface are shown schematically in 17. We have drawn the s and  $d_{z^2}$  contribution (and omitted  $p_z$ ), but really one has a linear combination of these, i.e., hybridization of the surface orbitals, in a chemically intuitive way, so as to produce hybrids reaching out for better interaction with n.

The discussion up to now has focused on the methyl n orbital. A consideration of the fragment overlaps and energies, the factors that determine the extent of interaction, would indicate other CH<sub>3</sub> orbitals should interact less. So they do. The CH<sub>3</sub> n orbital changes its occupation from 1.0 in free methyl to 1.52  $\rightarrow$  1.74 in various chemisorbed states (see Table III, a summary of CH<sub>3</sub> bonding characteristics calculated for the three metal surfaces and adsorption sites 6-8). The net charges for  $\pi$ -CH<sub>3</sub> and  $\pi^*$ -CH<sub>3</sub> are much smaller. Thus the depopulation of  $\pi$  is  $\leq 0.16$  and the population of  $\pi^*$  is  $\leq 0.11$  electron (these numbers are not in the table).



Interaction diagram 17 is highly schematic. Let us see the actual manifestations of the bonding on the DOS. We already saw the n peak move down in energy in the DOS decomposition of Figure 2. Now let us examine the detailed contribution of n,

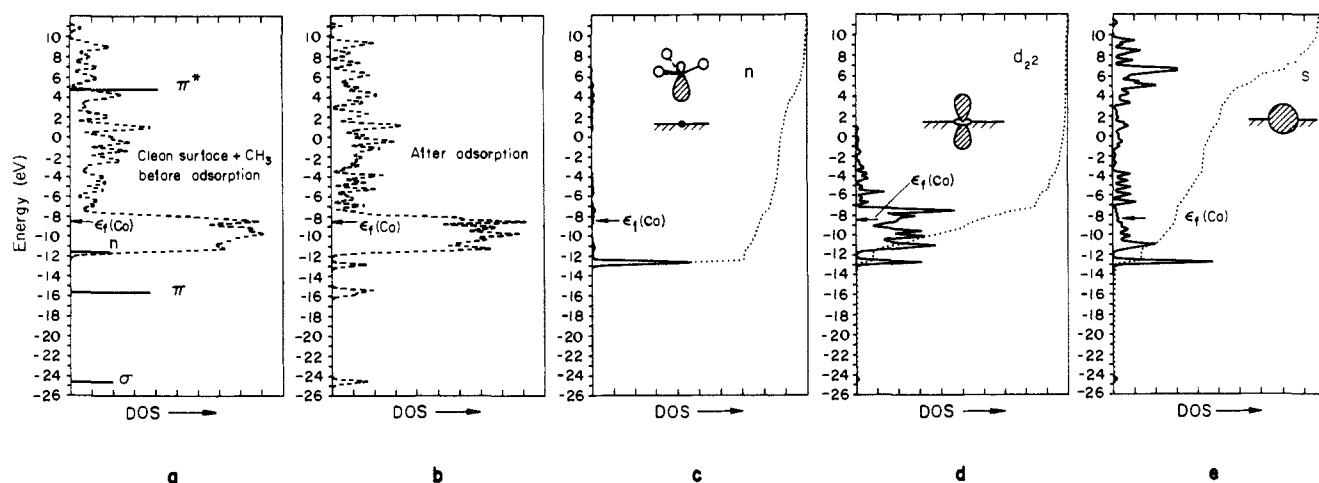


**Figure 3.** DOS of the chemisorbed Co(0001) ( $CH_3$  on-top). (a) DOS before the adsorption, the dashed line indicates the metal DOS, the horizontal lines show the free  $CH_3$  MO levels. (b) Total DOS after the chemisorption occurs. (c)  $n-CH_3$  (magnified) states in the chemisorbed system. Parts d and e show the  $d_{22}$  and  $s$  states (magnified), respectively, of the metal atom below the  $CH_3$  group.

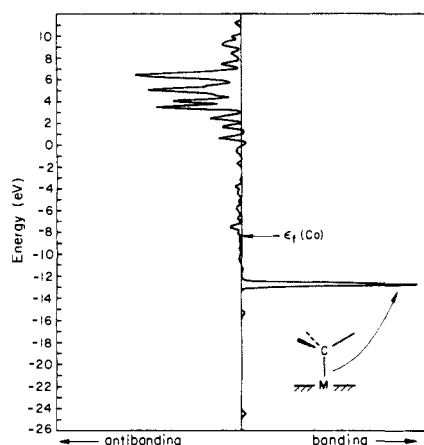


**Figure 4.** COOP curve of the  $M-C$  bond of a  $CH_3$  group on Co(0001) in the on-top geometry.

$s$ , and  $d_{22}$  to the DOS. This is shown in Figure 3, along with the COOP curve of Figure 4.

The peak in the DOS of the composite system at  $-13$  eV is mainly the methyl lone pair,  $n$ . It is stabilized by interaction with surface  $d_{22}$  and  $s$ . This is attested to by the contribution of these orbitals—10% of the total  $s$  states and 9% of the  $d_{22}$  states lie in this band (see projections in Figure 3)—and their predominant metal-carbon bonding character (see the COOP curve in Figure 4).

The antibonding component of the metal-methyl interaction is also clearly seen. The metal  $d_{22}$  band, formerly confined to the region of  $-12$  to  $-8$  eV, is now broader,  $-13$  to  $+2$  eV. Much of the density in it is pushed up above the Fermi level. The COOP curve shows a broad region of  $M-C$  antibonding from  $-11$  to  $-4$  eV. Here are disposed, highly delocalized,  $n-d_{22}$  antibonding combinations. The still higher energy  $M-C$  antibonding region arises from out-of-phase mixing of metal  $s$  and  $p_z$  with the methyl lone pair.

Some further insight into the special interaction of surface  $d_{22}$  may be obtained by looking at the contribution to the DOS of the surface Co atom *not* involved in bonding to a methyl group, Co2, and comparing it with the bonded Co1. This is done in Figure 5. Note how the Co2  $d_{22}$  DOS remains compact, relatively undispersed, while that of Co1  $d_{22}$  becomes quite spread out. Bonding implies dispersion.

We have now seen how the qualitative model of localized interactions and a perturbation theory based language for discussing these interactions are beautifully supported by the DOS and COOP curves. The molecule is bound to the surface primarily by the  $n + d_{22}$  interaction. Many  $M-C$  antibonding combinations are pushed above the Fermi level. The  $n$  band is substantially

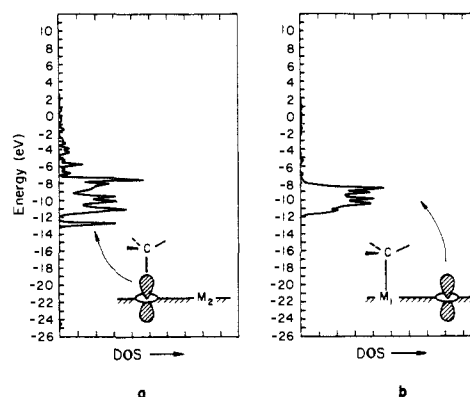


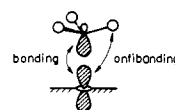
**Figure 5.** A comparison of the  $d_{22}$  states. Part a corresponds to the metal below the  $CH_3$  group and part b the adjacent metal atom (the one not capped by a  $CH_3$ ).

more than half populated, with 1.6 electrons per methyl group. Note that this brings the  $CH_3$  group closer to  $CH_3^-$ , but then the formalism of the methyl choice was just that, a formalism.

Another interaction that might have led to further charge transfer to  $CH_3$  is  $\sigma$  between various metal orbitals, mainly  $d_{xz}$ ,  $d_{yz}$ , and methyl  $\pi^*-CH_3$ . The calculations show clear signs of that interaction, but it is not very effective, for the separation in energy between the interacting orbitals is large.

We have discussed so far the  $M-C$  bonding, which is obviously the major chemical event that occurs when methyl is attached to a metal surface. However, there are additional bonding interactions between the metal and the organic fragment as well as changes within the metal slab and within the organic fragment. Let us discuss now briefly these "secondary" changes that follow adsorption.

Looking first at the hydrogen-metal interactions, we find that these are extremely small and slightly  $M-H$  antibonding. This holds for both the  $M1-H$  and ( $M1$  is the metal atom directly bonded to carbon, etc.) and the  $M2-H$  interactions. Thus, for Co, the corresponding overlap populations are  $-0.02$  and  $-0.00$ , respectively. A detailed examination of the COOP curve for  $M-H$  bonding shows an antibonding contribution in the band at  $-12.6$  eV, which is mainly the bonding  $n + d_{22}s$  combination. The small  $M-H$  antibonding effect is set by the phase relationship defined in 18.



Our conclusion that the M-H interactions are weak and unimportant contrasts with those of Muetterties' group.<sup>22</sup> They have performed extended Hückel cluster-type calculations<sup>22a</sup> and have reached the conclusion that multicenter metal-hydrogen-carbon interactions play a decisive role in the chemisorption of hydrocarbons on clean metal surfaces. They emphasized that the most stable geometries are those that achieve maximum multicenter bonding of this type. In light of this discrepancy we looked further into this problem. We changed the M-C-H angle from 109.5° to 95°, so that the Co1-H distance decreases from 2.67 Å in 6 to 2.45 Å. Still we find no indication of metal-hydrogen bonding. On the contrary, as the hydrogens approach the metal surface the antibonding interactions increase. Thus our calculations predict repulsion, not attraction, between the surface and the  $\beta$ -hydrogens. It is interesting that Minot, Van Hove, and Somorjai<sup>18</sup> used extended Hückel cluster calculations similar to those of Muetterties and did not mention the presence of strong metal- $\beta$ -hydrogen interactions.

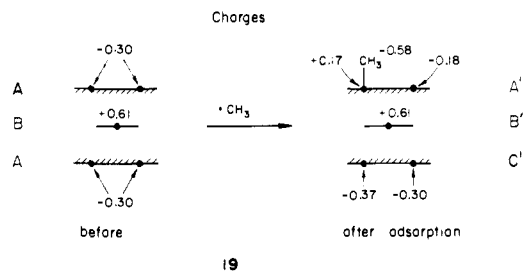
We now turn to the metal-metal bonding changes upon chemisorption of the methyl group. We find that as the new M-C bond is formed the metal-metal bonds around the binding site are weakened. Thus, the overlap population between Co1 and Co2 drops from 0.19 in the bare metal to 0.17 in the covered surface (similarly for Cr and Ti the values are 0.46 and 0.41, 0.35 and 0.29, respectively). To some extent the new M-C bond is formed at the expense of weakening the bonds within the metal lattice.<sup>21</sup>

The overall effect of adsorption on the C-H bonds is small. The relevant overlap population is 0.78 in isolated CH<sub>3</sub>, 0.79 in isolated CH<sub>3</sub><sup>-</sup>, and 0.79 for the Co surface.

Further insight into the bonding mechanism is provided by analyzing the charge distributions. The methyl is calculated to be strongly negative with a charge of -0.58. This is for Co. High negative values are observed for the other metal surfaces. Thus, if the metal and the CH<sub>3</sub> fragments are taken as neutral when separated, then upon chemisorption strong electron transfer from the metal to the methyl takes place; the metal becomes positively and the methyl negatively charged. This is true for Ti and Cr surfaces as well as Co, though there are differences to which we will return later.

Where does this electron transfer come from, and how can we reconcile it with the organometallic view of methyl as a donor? The electron transfer derives primarily from the large (80%) occupation of *n* on adsorption, and that in turn is a consequence of the *n* + *d*<sub>z<sup>2</sup>*s* bonding combinations, the large peak in the DOS at -12.6 eV, coming way below the Fermi level. To put it another way, and at the same time to answer the second question posed above, on the surface *n* is filled, and a better conceptual starting point might have been to think of it as an adsorbed CH<sub>3</sub><sup>-</sup>, a carbanion. If one views the charge transfer as beginning from CH<sub>3</sub><sup>-</sup> and (slab)<sup>+</sup> then the process of bonding is accompanied by a drift of 0.42 electron from CH<sub>3</sub><sup>-</sup> to the slab. The direction of this electron drift might make some organometallic chemists happier; we think what is important is that one perceives the equally valid dual viewpoints of the bonding process.</sub>

From which levels of the metal's "sea of electrons" do these transferred electrons come? We return here to a neutral CH<sub>3</sub> reference (i.e., the calculated transfer being to methyl). Examination of the electron distribution chart (for Co), 19, shows that most of the electrons (0.47 electron) come from one metal atom, Co1, which is directly bonded to the organic fragment. The adjacent atoms in the surface layer, Co1, also participate by donating 0.12 electron. The other atoms are merely spectators in the bonding process. The inner B and the bottom A layers remain essentially unchanged. The only atom in the inner layers that "feels" the adsorbent is the Co atom located exactly below Co1, which gains 0.07 electron. Interaction ④ in 10, which involves charge transfer within the metal slab, is small in this case.



Thus the charge transfer is a localized phenomenon, occurring mainly between the two atoms (Co1 and C) that form the new bond. Furthermore, not all the orbitals on Co1 contribute. Most of the charge comes from the *d*<sub>z<sup>2</sup> orbital (0.53 electron), and the *d*<sub>xz</sub> and *d*<sub>yz</sub> orbitals contribute only 0.002 electron each. The small electron donation from the *d*<sub>xz</sub> and *d*<sub>yz</sub> orbitals is a strong indication that the *p*-type interactions with  $\pi^*$ -CH<sub>3</sub> are relatively weak and charge transfer occurs mainly in the  $\sigma$ -framework through the M-*n* interaction (see 17). Thus, based on the charge criteria, M-C bonding is due mainly to the  $\sigma$  M + *n* interaction. Similar conclusion can be drawn for the Ti and Cr surfaces.</sub>

To summarize, the overall picture that emerges from our analysis is that of *localized* bonding where essentially only *one* metal atom participates in the formation of the new metal-CH<sub>3</sub> bond. The orbitals that participate are also limited. In the metal slab these are mainly *d*<sub>z<sup>2</sup> and *s* on M1 and on the methyl it is primarily the methyl lone pair, *n*. The other metal atoms as well as the other orbitals hardly feel the adsorbent. This bonding description is very similar to that in an isolated ML<sub>5</sub>CH<sub>3</sub> complex, of which many are known. There is one difference in the surface case. In the molecular case the ML<sub>5</sub> acceptor orbital that interacts with the CH<sub>3</sub> *n* is an empty *d*<sub>z<sup>2</sup>-*s*-*p*<sub>z</sub> hybrid, and that hybrid becomes populated upon interaction. In the case of the surface the orbital that interacts with CH<sub>3</sub> *n* is not one orbital, but the entire *d*<sub>z<sup>2</sup> band. The metal actually loses electron density through this interaction, as some *d*<sub>z<sup>2</sup>-*n* antibonding combinations are pushed above the Fermi level.</sub></sub></sub></sub>

Let us examine now how the bonding between the methyl and the surface changes as the electron count of the metal is decreased. Relevant overlap population data for Co, Cr, and Ti as well as the corresponding binding energies are presented in Table III.

As one sweeps across the transition series from left to right the average energy of a *d* electron, the center of gravity of the *d* band, moves down. This variation may have certain consequences, for as the center of gravity of the band shifts different adsorbate levels may interact more or less strongly. A good illustration of this may be found in another reaction we have studied, CO chemisorption and dissociation.<sup>19</sup> As one moves to the left in the transition series, the CO  $\pi^*$  becomes increasingly occupied, with consequent dissociative chemisorption.

According to the COOP curve of Figure 4, the *d* band energy range above the *n* peak is mainly M-C nonbonding. Thus as the *d* band is depopulated the M-C overlap population (which is summed up to the Fermi level) is expected to remain about the same. In the Ti case, however, the *d* band is higher in energy and should interact less effectively with *n* (by the energy criterion of eq 2). This is reflected in the M-C overlap populations that are listed in Table III.

The metal-metal overlap population increases on going from Co to Cr, as expected from the fact that the top of the *d* band is metal-metal antibonding. But from Cr to Ti some bonding states are emptied, so we expect the overlap population to decrease and the M-M bond to be weakened. Figure 6 shows a typical COOP curve for the M-M bond which is the basis of this reasoning.

The binding energies of the methyl fragment to the metal surface, which are also given in Table III, are naturally of special interest. The binding energy is defined here as the energy of a covered unit cell minus the combined energies of the neutral methyl fragment and of a unit cell of the bare surface. Although the extended Hückel method is not expected to reproduce quantita-

(22) (a) Gavin, R. M., Jr.; Reutt, J.; Muetterties, E. L. *Proc. Natl. Acad. Sci. U.S.A.* 1981, 78, 3981. (b) Muetterties, E. L. *J. Organomet. Chem.* 1980, 200, 177.



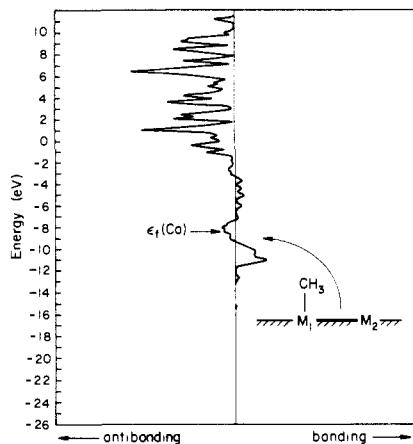
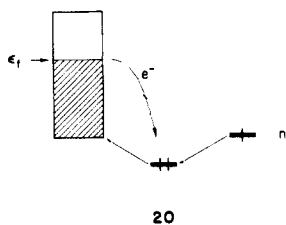


Figure 6. COOP curve for the surface M-M bond of the  $CH_3$  on the Co(0001) (on-top) system.

tively the binding energies we do believe that the relative binding energies have chemical significance.

We have traced down above the origins of the bonding interactions between the metal and the methyl. The binding energy gives the total energetic consequences that occur as the methyl binds to the surface. These include the changes that occur in all bonds, specifically the M-C, M-M, M-H, and C-H bonds. Why do the binding energies ( $E_1$ ) that are defined as  $E_1 = [E(\text{slab}) + E(CH_3)] - E_{\text{total}}$  decrease on going from Ti to Co although the M-C bonds get stronger and the M-M bonds alternate in the way we described above (Table III)? This apparent paradox is reminiscent of a similar situation that occurs in using frontier orbital arguments in analyzing the strength of simple two-electron bonds.<sup>23</sup> Within this simplistic theoretical framework it seems that the strength of a bond should increase as the energy separation between the interacting orbitals decreases, i.e., as its covalent character increases. Highly ionic bonds, where the separation between the orbitals that form the bonds is very large, are therefore expected to be extremely weak, contrary to reality.<sup>23</sup> As we use here essentially frontier orbital logic (eq 2) in analyzing the M- $CH_3$  bond, which on the basis of the charge distribution is substantially ionic, it is not surprising that similar problems arise. Picture 20 describes schematically the energetic consequences of



the ionic character of the M-C bond. The M-C bond strength arises mainly from the fact that the approaching  $CH_3$  radical brings along a "hole" at an energy of  $-11.75$  eV,  $3.26$  eV below the Fermi level of cobalt. The M-C bond is formed by an electron transfer from the metal into this "hole", and a binding energy of  $3.26$  eV is gained in this process. Thus, the "ionic character" of the M-C bond can be described as responsible for 87% of the total binding energy ( $3.73$  eV) of the methyl radical to the Co surface. The difference of  $0.47$  eV can be described as the "covalent contribution" to M-C bonding ( $E_2$  value in Table III, see also discussion below).

As we move from Co to Ti the Fermi level changes by  $2$  eV to higher energy. The energy gain on filling the "hole" is now greater (see 20), and so is the binding energy and charge transfer to the methyl ( $-0.59$  and  $-0.79$  for Cr and Ti, respectively). The smaller "ionic contribution" to the binding energy for Co compared to Ti is partially compensated by the increased "covalent character"

(23) Fleming, I. *Frontier Orbitals and Organic Chemical Reactions*; John Wiley & Sons: New York, 1976.

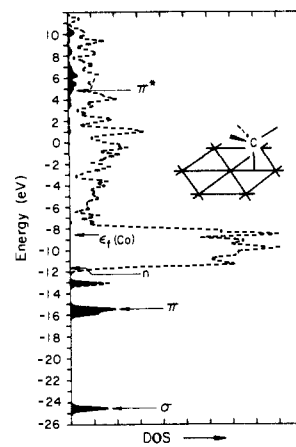


Figure 7. Total DOS (dashed line) and the  $CH_3$  contribution (darkened area) of the bridging  $CH_3 + Co(0001)$  system. The arrows indicate where the free  $CH_3$  MO levels were before the adsorption.

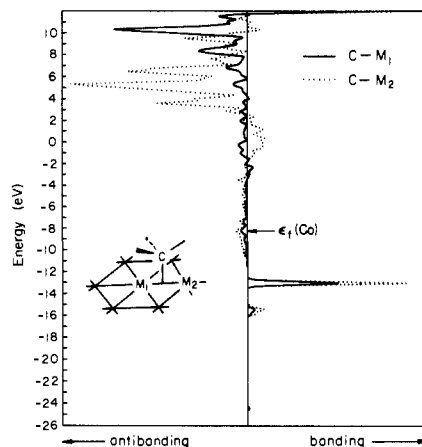
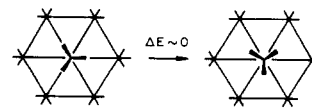


Figure 8. COOP curves of the two nonequivalent C-M bonds in the bridging  $CH_3 + Co(0001)$  system.

of the Co-C bond which is reflected in the increased M-C overlap population (Table III). The binding energy of methyl to Ti is therefore greater than that of Co- $CH_3$  by only  $1.7$  eV, not  $2$  eV as suggested in 20.

Once again it is useful to change perspective and think of the binding energy of a  $CH_3^-$  anion to a positively charged slab. The "hole" is filled and ambiguities of charge transfer are avoided. Now the binding energy  $E_2$ , defined as  $E_2 = [E(\text{slab}^+) + E(CH_3^-)] - E_{\text{total}}$ , is lower for Ti ( $0.16$  eV) than for Co ( $0.47$  eV), paralleling the M-C overlap populations. Cr is intermediate between Ti and Co; due to its nonhexagonal lattice it might deviate from average behavior.

A final point to be made about the on-top site is that the barrier for the rotation of the methyl group around its local  $C_3$  axis of symmetry (see 21) is nearly zero. This is hardly surprising, for this is a sixfold barrier, and we know such to be very small in molecular cases.



21

### The Bridging Methyl Geometry, 7

Figure 7 displays the total DOS (dashed line) of the Co(0001) system upon chemisorption of  $CH_3$  in a doubly bridging geometry. The darkened areas show the contributions of the organic fragment and the arrows indicate the location of these states in the isolated fragment. Figure 8 shows the COOP curves for the metal-carbon bonds. Comparison of Figures 7 and 3 and of 8 and 4 reveals

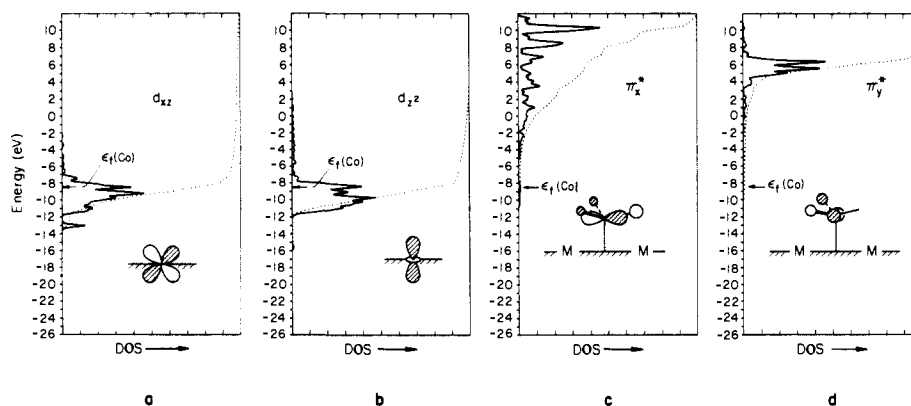
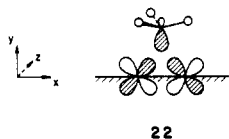


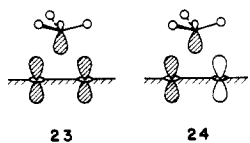
Figure 9. DOS of the bridging  $\text{CH}_3 + \text{Co}(0001)$  system: (a)  $d_{xz}$ ; (b)  $d_{yz}$ ; (c)  $\pi^*_x$ ; (d)  $\pi^*_y$ . The dotted lines are the integrations.

immediately the similarity in the bonding mechanisms in the on-top and the bridged geometries. In both cases the interaction that is primarily responsible for the metal-carbon bonding is that with the  $n$  orbital. Nevertheless, there are important differences in the details of the bonding mechanisms in the two geometries and we concentrate our attention on these.

The major difference is obvious. In the "on-top" geometry only one surface atom contributes strongly to  $\text{M}-\text{CH}_3$  bonding, while in the bridging case two metal atoms are clearly involved. More interesting is the contribution of the various orbitals to  $\text{M}-\text{C}$  bonding. In contrast to **6**, the carbon atom in **7** is located off the  $d_{xz}$  nodal plane and effective interaction with the  $n$  orbital can now occur, see **22** (contrast with **12**).



As seen in **22** these interactions take place with  $d_{xz}$  levels at or near the edge of the Brillouin zone, i.e., the bottom of the band. Projection of the  $d_{xz}$  levels (Figure 9a) indeed shows considerable broadening of this band compared with that of **6**. In the bridging geometry the  $d_{xz}$  band contributes 12% (6% for each of the Co atoms) of the total number of states in the  $n$  band at  $-13$  eV. In **6** (on-top) this contribution was close to zero. Another consequence of bridging is that  $n$  interacts effectively only with the bottom of the  $d_{yz}$  band (**23**), and not with the top (**24**).

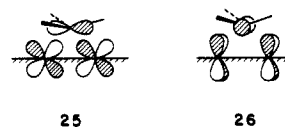


We thus expect that the contribution to  $\text{M}-\text{C}$  bonding from the  $d_{yz}$  band will be smaller in the bridging mode than in the on-top site. This is indeed observed. The contribution of the  $d_{yz}$  band to  $\text{M}-\text{C}$  bonding (i.e., its portion of the  $n$  peak in the DOS) drops from 9% in **6** to less than 2% in **7** (compare Figures 9b and 3d). The participation of the  $s$  band also diminishes from 16% in **6** to 12% in **7**.

The contribution of the  $\pi$ -type interaction to  $\text{M}-\text{C}$  bonding is higher in the bridging than the on-top site. This is indicated in Figure 8 by the increased contribution of the  $\pi-\text{CH}_3$  orbital at  $-15.3$  eV to  $\text{M}-\text{C}$  bonding (compare with Figure 4). A major difference between **7** and **6** is that in the former the degeneracy of the methyl  $\pi$ -interactions is destroyed. These are two distinct components, one pointing along the  $\text{M}-\text{M}$  axis (i.e.,  $x$  in **25**) and the other in a direction perpendicular to it ( $y$  in **26**). The  $\pi_x$  orbital interacts more strongly with the metal surface orbitals (see **25**) than the  $\pi_y$  orbital (see **26**). This is due primarily to the poorer orbital overlap in **26**, but also to the energy of the piece of the  $d_{xz}$  or  $d_{yz}$  band with which overlap is effective. The representative  $d_{xz}$  orbital is near the top of its band (see the nodal relationship

in **25**) and so closer in energy to its  $\pi^*-\text{CH}_3$  partner. The representative  $d_{yz}$  orbital is low in its band, **26**.

This effect is beautifully exhibited by comparing parts c and d of Figure 9, which show the projected DOS curves of the methyl  $\pi^*_x$  and  $\pi^*_y$  orbitals, respectively. While the  $\pi^*_x$  orbital is dispersed into a band of significant width indicating strong interaction with the metal, the  $\pi^*_y$  band remains relatively narrow.



The two bonded metal atoms contribute similarly, as expected, to the bonding of the  $\text{CH}_3$  fragment. This is apparent from the total  $\text{M}-\text{C}$  overlap populations shown in **27**, which indicate a slightly stronger  $\text{Co1}-\text{C}$  bond.  $\text{Co1}$  is "staggered" with respect to the methyl hydrogens and  $\text{Co2}$  is "eclipsed".

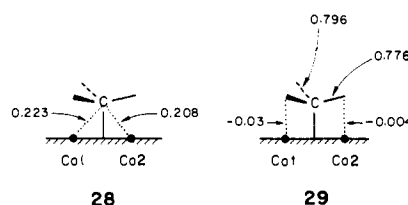
		Total			
Ti : 0.374		0.184		0.201	0.385
Cr : 0.418		0.227		0.209	0.436
Co : 0.414		0.224		0.208	0.432

27

Closer examination of the COOP curves in Figure 8 reveals an intriguing difference between  $\text{Co1}$  and  $\text{Co2}$ . The COOP peak corresponding to the  $\text{M} + n$  interaction is almost twice as large for  $\text{Co2}$  as for  $\text{Co1}$ . In the  $d$ -band region the contribution of  $\text{Co2}$  to  $\text{M}-\text{C}$  antibonding is also larger than that of  $\text{Co1}$ . For cobalt, where the  $d$  band is almost filled, the stronger contributions of  $\text{Co2}$  to  $\text{M}-\text{C}$  bonding and antibonding nearly compensate and the  $\text{Co1}-\text{C}$  and  $\text{Co2}-\text{C}$  overlap populations are similar, the former being somewhat larger. As the  $d$  band is depopulated the  $\text{M2}-\text{C}$  bond should gradually strengthen. The overlap populations calculated are in fact reversed for  $\text{M} = \text{Ti}$ , compared to  $\text{Co}$  (see **27**).

The stronger  $\text{M2}-\text{C}$  interaction, in particular in the  $n$  band, must result from the different arrangement of the methyl hydrogens with respect to the two relevant metal atoms. There is a correlated differential in the direct  $\text{M}-\text{H}$  and  $\text{C}-\text{H}$  overlap populations (see **28** and **29**). But the effect is small and we are not certain if it merits a detailed discussion.

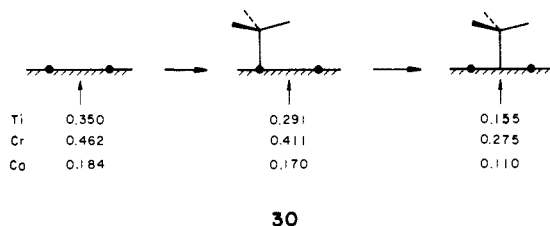
The total interaction between the methyl fragment and the metal surface seems stronger in the bridged geometry than in the on-top geometry. Thus, in **7** the  $\text{M} + n$  band that is the major



contributor to  $\text{M}-\text{C}$  bonding is pushed to a lower energy by 0.2

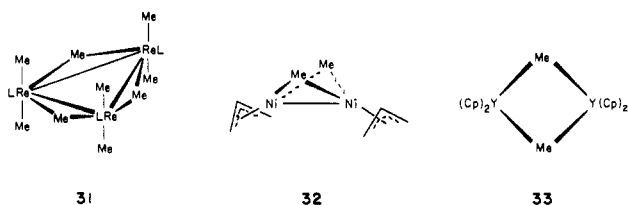
eV (for Co) relative to its position in **6**, indicating a stronger bonding interaction. Also, the M–C overlap population data indicate overall stronger M–C bonding in the doubly bridging site, **7**.

Although the bonding between the metal atoms and the methyl is stronger in the bridged geometry, the binding energy of the organic fragment to the surface is lower in **7** compared to that in **6** (see Table III). Thus, for Co, Cr, and Ti the binding energies of methyl in the bridging geometry are by 1.1, 0.9, and 0.5 eV, respectively, lower than in the on-top site. This apparent paradox of a stronger M–C bond that results in a weaker binding of the  $CH_3$  fragment to the surface becomes comprehensible upon examining the M–M overlap populations in **30**.

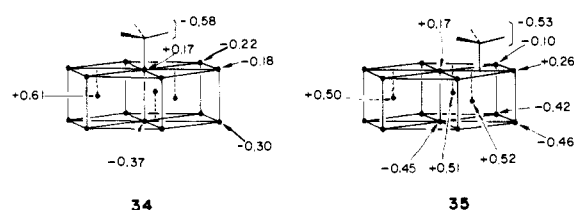


**30** shows that the M1–M2 bond is considerably weakened on going from **6** to **7**. This bond weakening is a direct consequence of the stronger metal–methyl interactions that push many of the metal bands to higher energies. The dominant n–d interaction pushes up above the Fermi level those metal states that contribute to either M–M bonding or M–M antibonding in the on-top geometry. But only M–M bonding states are lifted above the Fermi level by this interaction at the bridging position, and the M–M bond is weakened more. Thus, the stronger M–C bonding in **7** is gained at the expense of weakening the bonds within the metal slab, therefore raising its energy. In the Co case (and to a smaller degree also for Cr and Ti) the M–M bonding energy that is lost is greater than the M–C bonding energy that is gained upon bridging and the binding energy of methyl is lower in **7** than in **6**. In addition, interaction ④ in **10** plays a role: as the M–M bonding states are lifted up in energy, the electrons flow from these states into the top of the d band, which is M–M antibonding. Consequently, when the electron count on the metal decreases and the M–M antibonding states are depopulated the difference in binding energy between the on-top and the bridging geometry is reduced. In our calculation the difference is 1.1 eV for Co, 0.9 eV for Cr, and 0.5 eV for Ti, the on-top position being more stable.

Only a few molecular complexes are known that have a methyl group bridging two bonded metal atoms<sup>24</sup> (e.g., **31**<sup>24c</sup> and **32**<sup>25</sup>). In most such complexes the methyl bridges two nonbonded metal atoms, as in **33**.<sup>26</sup> Thus, it seems that in analogy to our computations for the covered surface, in the molecular complexes the bridging mode is accompanied by M–M bond weakening or by M–M bond cleavage.



Finally, we comment on the charge transfer that occurs upon bridging. This is shown in **34** and **35** for the cobalt surface.

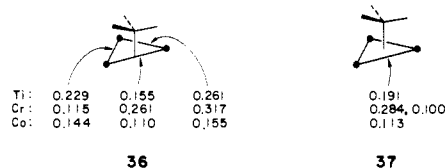


As we can see the total transfer of charge from the metal to the methyl fragment is nearly the same in **6** and **7** (0.58 and 0.53 electron, respectively). However, there appear to be dramatic changes in the charge distributions within the metal slab on going from **6** to **7**. There is a substantial flow of charge from the surface layer into the inner layers upon methyl bridging. The same is observed for Cr and Ti surfaces. Thus for cobalt the calculations show that on going from **6** to **7** the surface A layer loses 0.52 electron while the B and bottom A layers gain 0.30 and 0.36 electron, respectively. Thus, the Co surface layer which in the bare metal is negatively charged becomes nearly neutral for on top bonding and turns positively charged in the bridging case. This substantial charge flow away from the surface is easily understood in terms of the bonding picture that emerged from our calculations. Bridging involves stronger interactions with the metal d bands. The surface bands that are involved in these interactions are pushed up to higher energies and are therefore emptied. Charge flows to lower metal bands that are concentrated in the inner slab layers. These charge flows provide a clear determination of the importance of interaction ④ in **10**.

As in the on-top geometry, so also in the bridging site the methyl is essentially freely rotating; there is no calculated rotational barrier.

### The Threefold Bridging or Capping Methyl Geometry, **8**

Once we have analyzed in detail the on-top and the bridged geometries and have understood the bonding mechanism, then it is easy to predict what happens in the capping geometry **8**. The trends that have been observed on going from **6** to **7** will hold also for moving from **7** to **8**. In **8** the interactions between the methyl and the metal slab are the strongest, and the total M–C bonding increases, as expected, on going from **7** to **8**. **36** and **37** show the overlap populations for the M–C and M–M bonds in both geometries. Concurrently on going from **7** to **8** the M–M bonds are weakened as reflected in the decreasing M–M total overlap populations (see **36** and **37**). At high electron counts this results in a smaller binding energy for the capping geometry relative to the on-top mode (e.g., by 0.3 eV for Cr). For lower electron counts, many of the M–M bonding states, which are pushed up above the Fermi level by the  $CH_3$ –metal interaction, were originally empty. The gain in M–C bonding thus compensates more the loss in the M–M bonding in the lower electron count case. On the Cr surface our calculation shows no energetic difference between the bridging and capping sites and on Ti the capping geometry is more stable by 0.4 eV. In all cases under consideration, however, the on-top mode is the most stable one for  $CH_3$ .



The charge distributions also behave as expected. There is substantial electron flow from the surface layer into the inner metal layer. The charge on the methyl fragment decreases as its coordination number increases on the Co surface. Thus on the Co surface the  $CH_3$  charge is  $-0.58$  in **6**,  $-0.53$  in **7**, and  $-0.52$  in **8**. This trend can also be rationalized within our bonding model by using the following reasoning: If there is no interaction between the metal and the  $CH_3$  radical and the electrons are assigned to the lowest available levels, then the methyl's n orbital, which is lower in energy than the metal's d band, will be doubly occupied and the charge distribution is  $CH_3^-[\text{metal slab}]^+$ . When the

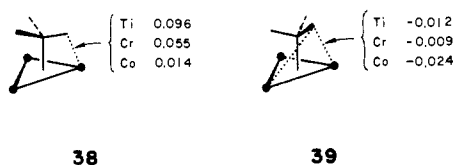
(24) (a) Hursthouse, M. B.; Malik, K. M. A.; Sales, K. D. *J. Chem. Soc., Dalton Trans.* **1978**, 1314. (b) Mertis, K.; Edwards, P. G.; Wilkinson, G.; Malik, K. M. A.; Hursthouse, M. B. *J. Chem. Soc., Dalton Trans.* **1981**, 705. (c) Masters, A. F.; Mertis, K.; Gibson, J. F.; Wilkinson, G. *Nouv. J. Chim.* **1977**, *1*, 389. (d) Edward, P. G.; Mertis, K.; Wilkinson, G.; Hursthouse, M. B.; Malik, K. M. A. *J. Chem. Soc., Dalton Trans.* **1980**, 334.

(25) Krüger, C.; Sekutowski, J. C.; Berke, H.; Hoffmann, R. *Z. Naturforsch.* **1978**, *33b*, 1110.

(26) Holton, J.; Lappert, M. F.; Ballard, D. G. H.; Pearce, R.; Atwood, J. L.; Hunter, W. E. *J. Chem. Soc., Dalton Trans.* **1979**, 54.

M-CH<sub>3</sub> interactions are "turned on", part of the methyl charge is transferred back to the metal. As the number and efficiency of the interaction mechanisms increases, as is the case along the progression 6 → 7 → 8, more charge is transferred back to the metal and the organic fragment becomes less negative.

The capping or triply bridging geometry is the first where we find a significant barrier of 6.3, 21.2, and 21.7 kcal/mol (for Co, Cr, Ti) for the rotation of the methyl group. The most stable arrangement is such that the hydrogens point toward three metal atoms. A top view is shown in 38. The less stable arrangement in which the hydrogens point toward the center of three M-M bonds is shown in 39. The M-H overlap populations that are given in 38 and 39 suggest that weak M-H attractive interactions favor

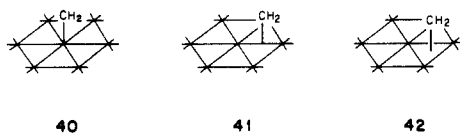


38 over 39, where these interactions are repulsive. 38 is the only case where we find some indication for the attractive M-H forces that Muetterties and co-workers found to be significant.<sup>22</sup> The larger rotational barrier at lower electron count is due to the following fact: At the eclipsed geometry 38 the hydrogens of the CH<sub>3</sub> group interact with both M-M bonding and antibonding states, whereas in the staggered 39 they interact only with the M-M bonding states. Thus 38 is more stable. At lower band filling it is more so because the unfilled M-M antibonding states act as acceptors. However, we are not sure whether the extended Hückel method has overestimated the barrier, so better calculations are needed.

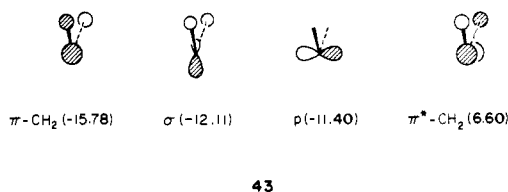
To conclude this section we summarize the main features of the bonding between a methyl fragment and the metal slab. The major interactions occur between the metal's surface bands and the CH<sub>3</sub> orbital. These interactions are  $\sigma$  type, involving surface  $d_{z^2}$  and  $s$  orbitals. The important difference from a molecular complex is that charge transfer in the  $\sigma$  system occurs from  $d_{z^2}$  (and  $s$ ) to CH<sub>3</sub>. But this is a consequence of the reference state as neutral CH<sub>3</sub>, and if CH<sub>3</sub><sup>-</sup> is chosen instead, the methyl group behaves in the way we would have expected. As one moves along the geometry series on-top → bridged → triply bridging, some additional M-C bonding is gained, but this is generally achieved at the expense of considerable weakening of the metal-metal bonds in the surface layer. As a result the on-top geometry is the most stable geometry for all three metal surfaces. However, this theoretical conclusion is not uncontested: see the theoretical work of Shustorovich<sup>36c</sup> and the experimental finding of a soft CH mode in CH<sub>3</sub> on Ni(111), indicative of a possible capping geometry.<sup>11b</sup>

#### Adsorbed Methylene

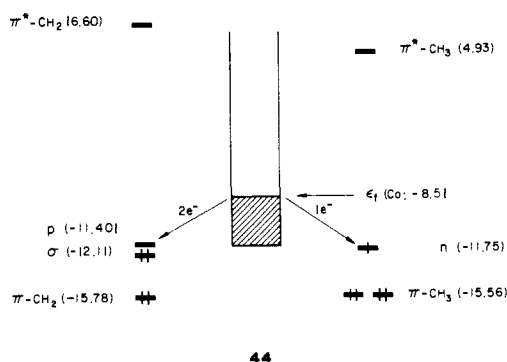
We will follow the guidelines of our analysis for the methyl case. As in the methyl system three adsorption sites are studied: the 1-fold on-top geometry 40, the 2-fold bridging position 41, and the 3-fold bridging or capping position 42. For each of these geometries two conformers with respect to rotation around the C<sub>2v</sub> axis of the methylene group were examined.



The major difference in the bonding of methyl and of methylene to the metal surface lies on the different set of orbitals that these two fragments bring to the bonding process. The relevant orbitals of methylene are displayed in 43 in increasing order of energy (in parentheses, eV) from left to right. In the free singlet methylene only  $\pi$ -CH<sub>2</sub> and  $\sigma$  are occupied. Note that for consistency with the methyl case we should have called the lone pair orbital  $n$ , but it is customary to designate it as  $\sigma$  in carbene chemistry.

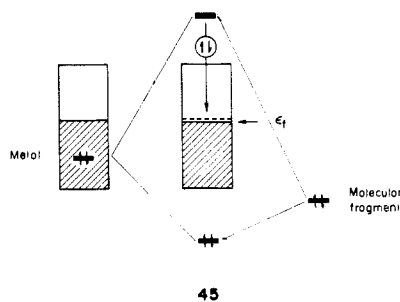


A schematic energy diagram of the methylene orbitals and the metal slab levels is displayed in 44. 44 also shows the position of the relevant orbitals of the methyl radical.



Let us examine first the most important features of the surface-carbene bonding, those which hold for all the binding sites. Diagram 44 reveals at a glance the important differences in the bonding of methyl and methylene to the surface. The methyl fragment carries a singly occupied empty orbital at -11.75 eV while the methylene introduces an entirely vacant orbital at a similar energy. We have seen above that most of the binding energy of the organic fragment to the metal surface can be associated with the "ionic character" of the M-C bond, in other words with the energy gained upon filling the "hole" that the organic fragment is carrying. Using this naive picture we expect that methylene, which carries 2 empty sites, should be bound much more strongly to the surface than methyl, which provides only one vacancy. Note also that the empty orbital that methylene brings along is the  $p$  or  $\pi$ -type while that of methyl is of  $\sigma$ -type. The bonding of methylene to the metal surface is therefore expected to have a much more pronounced  $\pi$ -character than that for methyl. We will see below that these qualitative expectations are indeed fulfilled.

Another important difference between methyl and methylene is that in CH<sub>2</sub> the  $\sigma$  orbital is doubly occupied while in CH<sub>3</sub> it is singly occupied. This orbital interacts mainly with filled metal levels (see 44). When two filled orbitals interact this results in a strong destabilization due to the occupation of antibonding orbitals. This would have indeed been the case for the interaction of the  $\sigma$  orbital of CH<sub>2</sub> with a filled orbital of another molecular fragment. However, the situation in the metal slab is entirely different. The electrons that should enter the antibonding states can instead occupy empty metal levels that are lying near the Fermi level. These states, which we have shown above to be primarily bulklike, serve as an empty reservoir for electrons that are pushed up by interactions between filled levels. These arguments are displayed schematically in 45.



The strong destabilization that is associated with 4-electron interactions in molecules, and that controls much of their

Table IV. Energetics and Electron Redistribution upon Methylene Bonding

		Fermi level (eV)	binding energy (eV)		orbital populations		charge on $CH_2$	overlap populations			
			$E_1$	$E_2$	$\sigma$	$p$		$M_1-M_2$	$M_1-C$	$M_1-H_1$	$C-H_1$
	Ti	-6.49	10.38	0.64	1.70	1.89	-1.59	0.29	0.55	-0.04	0.81
	Cr	-7.60	8.02	0.42	1.64	1.90	-1.53	0.40	0.52	-0.04	0.80
	Co	-8.50	6.33	0.52	1.59	1.96	-1.54	0.17	0.44	-0.02	0.79
	Ti	-6.44	9.94	0.20	1.69	1.78	-1.46	0.15	0.28	-0.03	0.81
	Cr	-7.45	7.15	-0.45	1.62	1.81	-1.40	0.24	0.28	-0.03	0.79
	Co	-8.47	5.31	-0.50	1.55	1.86	-1.37	0.11	0.23	-0.03	0.79
	Ti	-6.46	10.40	0.66	1.69	1.72	-1.42	0.14	0.42	-0.04	0.81
	Cr	-7.53	8.13	0.53	1.60	1.69	-1.29	0.25	0.43	-0.03	0.80
	Co	-8.48	6.35	0.54	1.53	1.64	-1.17	0.10	0.40	-0.02	0.80
	Ti	-6.46	10.05	0.30	1.69	1.70	-1.39	0.15	0.18 <sup>a</sup>	-0.01	0.80
	Cr	-7.43	7.49	-0.11	1.60	1.64	-1.22	0.27	0.16 <sup>a</sup>	-0.00	0.78
	Co	-8.47	5.75	-0.06	1.53	1.62	-1.12	0.11	0.17 <sup>a</sup>	-0.02	0.79

<sup>a</sup>The  $M_2-C$  overlap populations are 0.35, 0.36, and 0.33 for Ti, Cr, and Co, respectively.

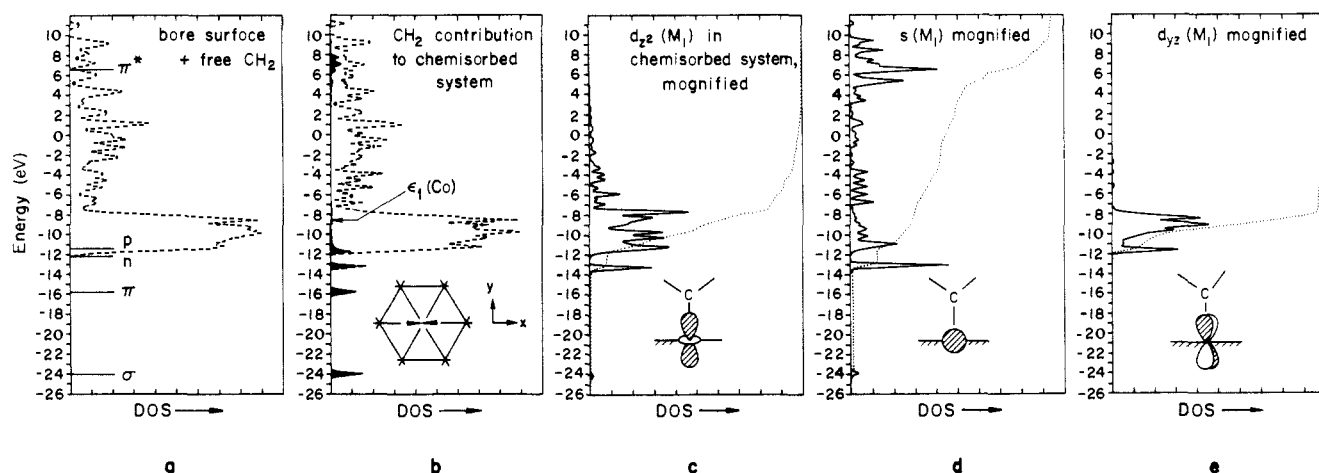


Figure 10. DOS of the on-top  $CH_2 + Co(0001)$  system: (a) Bare metal surface (dashed line) plus free  $CH_2$  (MO levels indicated by horizontal lines); (b) Total DOS (dashed line) and the  $CH_2$  contribution (darkened area) for the chemisorbed system; (c)  $d_{z^2}$  states of the metal atom bonded to the  $CH_2$  group (magnified); (d)  $s$  states (magnified); (e)  $d_{yz}$  states (magnified).

chemistry, has to a large extent diminished in metal-adsorbent systems. This is, we believe, one of the important characteristics of metals and metal surfaces, a factor that makes them behave so differently from the "analogous" isolated metal complexes.

We can proceed now to discuss in detail the different binding sites of methylene. Table IV collects the computational data regarding the bonding characteristics of methylene in the different adsorption sites. Some of these data will be discussed in some detail in the text. We also refer the interested reader to a recent contribution from our group in which we studied the adsorption of vinylidene,  $H_2C=C$ , on metal surfaces.<sup>21</sup> In many aspects this system is similar to ours and we will refer to it when appropriate.

#### Adsorbed Methylene in the 1-Fold On-Top Geometry, 40

We have studied two conformers shown in 46 and 47 differing by a  $30^\circ$  rotation around the metal-carbon bond. We find that the energy difference between these conformers is essentially zero. We will comment on the reasons for this tiny barrier later. We concentrate therefore on one geometry, 46, using the indicated coordinate system, but the analysis applies to 47 as well.

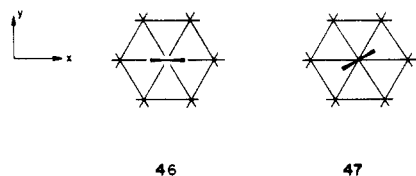


Figure 10a,b shows the total DOS curve (dashed line) of the Co system before and after the chemisorption of  $CH_2$  in this geometry. The dark area in Figure 10b gives the states contributed by the methylene fragment and the straight lines in Figure 10a

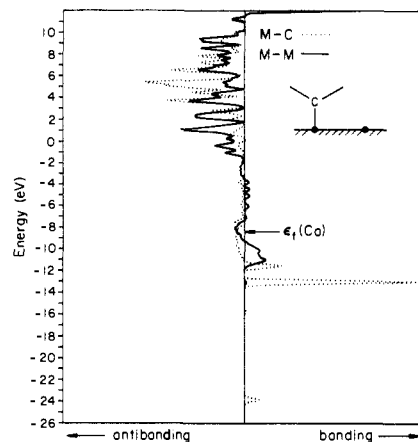


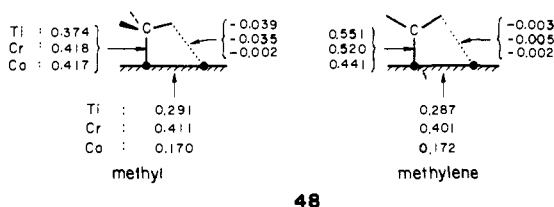
Figure 11. COOP curves of the M-M (solid line) and the C-M (dotted line) bonds for the on-top  $CH_2 + Co(0001)$  system.

indicate the location of these states in the isolated organic fragment. Figure 10b can be compared with the analogous Figure 2a for the 1-fold chemisorbed methyl. The two orbitals of methylene that are most affected by the interaction with the metal are  $\sigma$  and  $p$ . These are pushed to lower energies by 1.2 and 0.4 eV, respectively. The peak of the  $\sigma$  band is located at a slightly lower energy in 46 than in 6. This is due primarily to the fact that  $\sigma-CH_2$  is lower than  $n-CH_3$  to start with (-12.1 vs -11.8 eV).

The fact that the  $\sigma$  orbital is affected more strongly than the  $p$  orbital by interaction with the metal indicates that the M-C bond is mainly of  $\sigma$  character. This interpretation is corroborated by Figure 11 which displays the COOP curve for the  $Co_1-C$  bond.

The strongest M-C bonding peak is at -13.0 eV corresponding to the  $\sigma$  orbital of methylene. The p orbital also makes an important contribution to M-C bonding, as indicated by the peak at -11.2 eV. But it does so to a smaller degree than the  $\sigma$  band.

Comparison of Figure 11 with the analogous COOP curve for methyl (Figure 4) is interesting. There are essential similarities, and small differences: the absence of a p bonding contribution in Figure 4, minor and understandable differences in the contribution of the  $\pi$  orbitals. Note also that around the Fermi levels of Co( $d^9$ ) indicated by the arrow in Figure 11, the M-C COOP curve is antibonding and it is more so for methylene than in the methyl system. Thus as the top of the d band is depopulated the M-C bond is strengthened. The M-C overlap populations are in agreement: 0.44 for Co, 0.52 for Cr, and 0.55 for Ti (Table IV). As in the methyl case, for methylene the M-M COOP curve (which is also shown in Figure 11) is also antibonding around the Fermi level of Co. Emptying the top of the metal band results therefore in a strengthening of the M-M bond, up to a certain point ( $\sim d^5$ ), past which it is weakened. The calculated overlap populations for the on-top methyl and methylene geometries are shown in 48 (see also Table IV). Note that also for methylene the M-H interactions are weakly antibonding.



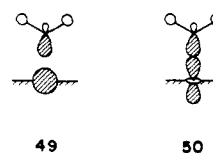
The calculated total overlap populations in 48 indicate that the M-C bond is stronger for methylene than for methyl. This comes from the increased contribution of  $\pi$  bonding. The difference in the overlap populations between the two cases is, however, too small to indicate the presence of a fully developed M-C double bond character. Qualitatively, the M-CH<sub>2</sub> bond is best described as a partial double bond.

The relatively modest increase in the M-C overlap population, and thus in the M-C bond strength, upon substitution of methyl by methylene does not indicate, as we have already emphasized earlier, that the binding energies of these fragments to the metal surface are similar. This is because the overlap populations reflect only what we have termed the "covalent" fraction of the bonding ( $E_2$ ) while most of the binding energy comes from an "ionic" transfer of electrons from the metal to the organic fragment. For the adsorption of CH<sub>2</sub> on cobalt we calculate a binding energy of 6.33 eV compared with only 3.73 eV for methyl. These values agree well with our interpretation. The "ionic" binding energy is given by the energy difference between the top of the bare cobalt band and the  $\sigma$ -orbital "hole", multiplied by 2 (for 2 electrons), i.e.,  $2 \times (11.40 - 8.48) = 5.84$  eV. The remaining fraction of the binding energy,  $6.33 - 5.84 = 0.49$  eV, can be associated with the "covalent" bonding. For methyl, only one electron contributes to the "ionic" stabilization, i.e.,  $11.75 - 8.48 = 3.27$  eV, and the total binding energy is only 3.73 eV (leaving 0.46 eV for "covalent" stabilization), roughly half that of methylene.

On going from Co to Cr to Ti, the Fermi level becomes higher and the "ionic" energy gain is larger, increasing the total surface-adsorbent bonding interactions (see  $E_1$  values in Table IV). The "covalent" bonding remains, as expected, roughly the same as the metal is altered (see  $E_2$  values in Table IV).

Now that we have discussed the general features of the bonding of CH<sub>2</sub> to the metal surface let us analyze the bonding of CH<sub>2</sub> to the metal surface in more detail. We have shown using Figures 10 and 11 that M-C bonding is associated mainly with the  $\sigma$  and p orbitals of CH<sub>2</sub>. Which of the metal levels contribute more to the M-C bond?

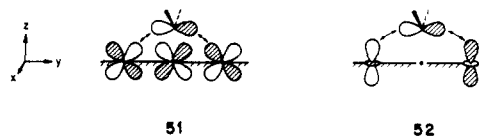
Interactions with the  $\sigma$  orbital of CH<sub>2</sub> involve mainly the metal's s and  $d_{z^2}$  bands as shown in 49 and 50, respectively. Interactions 49 and 50 are analogous to the  $\sigma$  interactions with the methyl fragment shown earlier in 11.



As for adsorbed CH<sub>3</sub>, so also for CH<sub>2</sub> essentially the entire s and  $d_{z^2}$  bands are involved in the interaction. This is the reason that we do not show the orbital phases at the neighboring metal atom. Projection of the  $d_{z^2}$  states of Co1 shown in Figure 10c reveals that nearly 8% of these states contribute to the metal- $\sigma$  band. For the s bands (Figure 10d) the contribution is slightly larger (12%). The strong interaction of the  $d_{z^2}$  band with the organic fragment is also evident from its large dispersion; nearly 40% of the  $d_{z^2}$  states are above the Fermi level of cobalt.

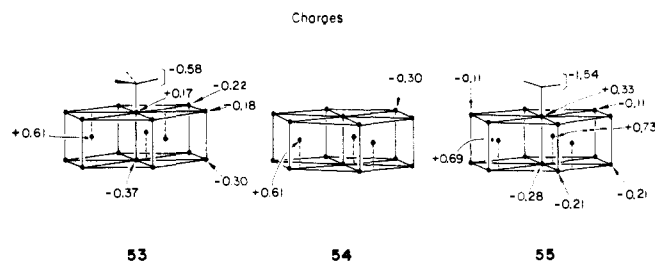
The p orbital of CH<sub>2</sub> can interact with several metal bands. The major interaction is with the  $d_{yz}$  levels as shown in 51. According to Figure 10e, 17% of the  $d_{yz}$  states are involved in  $\pi$  interactions with the p orbital. The neighboring metal atoms also contribute, as emphasized in 51 by the arrows. The  $d_{xz}$  levels, being perpendicular to the p orbital, do not interact with the organic fragment (except for a minor interaction with the  $\pi^*$ -CH<sub>2</sub> orbital, which is of proper symmetry but lies 18 eV above the p orbital). Some levels around the center of the  $d_{z^2}$  and s bands can also contribute to  $\pi$  bonding, as shown for  $d_{z^2}$  in 52. These interactions, however, do not in fact contribute much to the total  $\pi$  bonding, because of poor orbital overlap. Only 1-2% of the  $d_{z^2}$  levels contribute to the M-p band.

We can now understand why the barrier to the rotation of the CH<sub>2</sub> group is so small. The  $\sigma$ -type interactions are invariant to rotation of the CH<sub>2</sub> group and are the same in 46 and 47. The



important interactions for the rotation are the  $\pi$  type. As the CH<sub>2</sub> fragment is rotated toward geometry 47 the contribution of the  $d_{yz}$  bands to  $\pi$  bonding decreases due to smaller orbital overlaps. However, at the same time the contribution of the  $d_{xz}$  bands (which are zero in 46) increases and reaches its maximum in geometry 47. A nearly constant contribution of these levels to the M-C bonding is maintained as the CH<sub>2</sub> fragment rotates. The rotation barrier is sixfold and tiny. The different effectiveness of the  $\sigma$  and  $\pi$  interactions is manifested also in the appropriate metal DOS.

In 55, we look at the charge distribution in the adsorbed methylene. We find two comparisons to be useful, one with the bare metal 54 and the other with the analogous 1-fold on-top methyl system 53. The data in 53-55 are for the Co surface, and data for other electron counts can be found in Table IV. As the CH<sub>2</sub> fragment provides two vacancies for the metal electrons while the methyl provides only one, the charge transfer to the organic fragment is much higher in the methylene system. The CH<sub>2</sub> charge is -1.54 compared with -0.58 for CH<sub>3</sub>. Using the adsorbed methyl system as the reference point we calculate that abstraction of a hydrogen atom causes 0.90 electron to flow from the metal



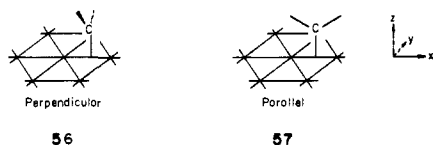
to the organic fragment. The charge is donated roughly equally from all three metal layers. Comparison with the bare surface shows that as in the methyl system, the charge that is donated to the methylene comes mainly from the Co atom that is directly

bonded to it. This cobalt atom contributes 0.64 electron. However, the electron demand placed by the methylene fragment is so large that the neighboring atoms in the surface layer as well as metal atoms in the bulk also contribute. The metal atoms adjacent to the adsorption site contribute 0.19 electron each and those in the B and bottom layers 0.32 and 0.20 electron, respectively. In the methyl case charge transfer from the inner metal layers is very small (see 19).

Numerous examples of carbene complexes of type 40 either substituted or unsubstituted are known.<sup>1a,12</sup> Their bonding was analyzed in detail by our group<sup>27a-d</sup> as well as by others,<sup>27e,f</sup> and we will not dwell on this point here. The reader is also referred to a recent relevant paper which reports the preparation and the characterization of the first simple unligated carbene complex  $FeCH_2$ .<sup>28</sup> Note, however, that to our best knowledge there is not a single known structure of a cluster carbene complex of type 40. These complexes exist commonly in a bridged geometry but 1-fold structures have been suggested as intermediates in their reactions.<sup>29-31</sup>

#### Adsorbed Methylene: The Twofold Bridged Geometry, 41

We have studied two bridged geometries, perpendicular 56 and parallel 57. It is advantageous to analyze these geometries together although they differ substantially in energy, 56 being lower in energy. We will come back to this point later.



As in the 1-fold geometry it is useful to discuss the metal-methylene bonding in terms of  $\sigma$  and  $\pi$  contributions. The  $\sigma$  interactions are expected to be similar in the two geometries, as those interactions remain reasonably invariant to rotation around the  $z$  axis. Furthermore, in comparison to the on-top geometry 40, the changes in the  $\sigma$  bonding are expected to be similar to that that occur in the methyl systems, i.e., 6  $\rightarrow$  7. For the  $\sigma$  framework we indeed find strong similarities between the methyl and the methylene systems. In both systems  $\sigma$  interactions are stronger in the bridged geometry.

The total density of states for methylene on Co(0001), bridging in the perpendicular conformation 56, is shown in Figure 12. The total DOS for the parallel conformation is similar, though it differs in critical aspects to be discussed below. Decompositions of the DOS identify methylene levels. Note that both  $\sigma$  and  $p$  bands are stabilized in the adsorbate-surface complex.

The dramatic difference between perpendicular and parallel geometries, 56 and 57, is revealed in the metal-carbon COOP curves which are displayed in parts a and b of Figure 13 for 56 and 57, respectively. Note that in contrast to 7, here symmetry dictates identical COOP curves for Co1-C and Co2-C, of which only one is shown. The contribution of states descending from the methylene  $p$  state to M-C bonding is approximately twice as great in 56 as in 57. In the perpendicular geometry the M-C bonding is roughly half  $\pi$  and half  $\sigma$  in character while in the parallel geometry  $\sigma$  bonding is dominating.

The stronger  $\pi$  bonding in 56 compared with 57 results from a more efficient overlap in the perpendicular geometry between

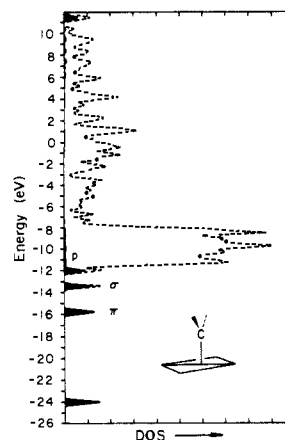
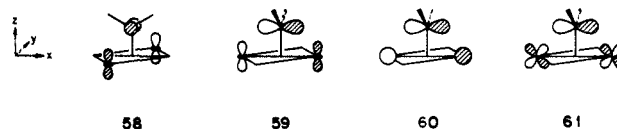


Figure 12. Total DOS (dashed line) and the  $CH_2$  contribution (darkened area) for the bridging  $CH_2 + Co(0001)$  system ( $CH_2$  perpendicular to the Co-Co bond, i.e., 56).

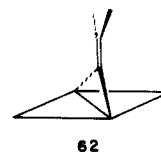
the  $p$  orbital and the appropriate metal states. In the parallel conformation the overlap between the carbene's  $p$  orbital and the top of the  $d_{z^2}$ , for example, is poor (see 58) so that there is practically no contribution of  $d_{z^2}$  to the  $p$  band. In the perpendicular geometry, on the other hand, overlap is excellent (see 59) and 6% of the  $d_{z^2}$  states contribute to the M- $p$  bonding band. Other metal states that contribute significantly to  $\pi$  bonding are the top of the  $s$  band ( $\sim 5\%$ , see 60) and the top of the  $d_{x^2-y^2}$  band ( $\sim 1\%$ ).  $d_{xz}$  also contributes, although its share is very small ( $\sim 2\%$ , see 61). The stronger  $\pi$  interaction in the perpendicular geometry is reflected in the greater M-C overlap populations. Accompanying this is a weakening of the bridged M-M bond, but the magnitude of that effect is small (see Table IV).



The stronger M-C bonds in 56 suggest that this conformation should be more stable than 57, as observed. For all metal surfaces we calculate substantial energy differences between the two conformations (ca. 1.0 eV for Co and Cr and ca. 0.5 eV for Ti). Note that these energy differences also give the barriers for rotation of the  $CH_2$  group around the  $z$  axis. It is interesting to note that these barriers are similar in magnitude to those found in molecular carbene complexes of the 1-fold type.<sup>27,29,30</sup> This similarity is not surprising because the key orbital interaction that dictates the magnitude of these barriers is similar in the molecular and the surface systems.

Our result that the perpendicular geometry is substantially more stable than the parallel geometry agrees with that of Minot et al.<sup>18a</sup> but is in contrast to the conclusions reached by Muettterties et al.,<sup>22</sup> who suggested that the parallel geometry is favored by strong metal-hydrogen interactions. As in the previously discussed systems, we find small antibonding interactions between the metal and the hydrogens in either 56 or 57 and for all electron counts (Table IV). Note that our results are in line with the known structures of analogous bridged molecular complexes, which invariably have a perpendicular geometry with respect to the bridged M-M vector. Relevant molecules can be found in ref 1a and 12.

It is interesting to compare our results with those of Silvestre and Hoffmann, who have found that the related vinylidene ( $CH_2=C:$ ) binds to a Pt surface most strongly in the parallel geometry 62.<sup>21</sup> The corresponding perpendicular conformation is substantially higher in energy. Although at first glance this



(27) (a) Lauher, J. W.; Hoffmann, R. *J. Am. Chem. Soc.* **1976**, *98*, 1729. (b) Goddard, R. J.; Hoffmann, R.; Jemmis, E. D. *J. Am. Chem. Soc.* **1980**, *102*, 7667. (c) Hoffmann, R.; Wilker, C. N.; Eisenstein, O. *Ibid.* **1982**, *104*, 632. (d) Eisenstein, O.; Hoffmann, R. *Ibid.* **1981**, *103*, 5582. (e) Rappe, A. K.; Goddard, W. A., III *Ibid.* **1980**, *102*, 5114; **1982**, *104*, 448. (f) Kostić, N. M.; Fenske, R. F. *J. Am. Chem. Soc.* **1982**, *104*, 3879.

(28) Chang, S.-C.; Kafafi, Z. H.; Hauge, R. H.; Billups, W. E.; Margrave, J. L. *J. Am. Chem. Soc.* **1985**, *107*, 1447.

(29) Dyke, A. F.; Knox, A. R.; Mead, K. A.; Woodward, P. *J. Chem. Soc., Chem. Commun.* **1981**, 861.

(30) (a) Laws, W. J.; Puddephatt, R. J. *J. Chem. Soc., Chem. Commun.* **1983**, 1020. (b) Holmgren, J. S.; Shapley, J. R. *Organometallics* **1985**, *4*, 793.

(31) For the structure of surface-bonded  $CH_2$  see, for example: (a) Demuth, J. E.; Ibach, H. *Surf. Sci.* **1978**, *78*, L238. (b) McBreen, P. H.; Erley, W.; Ibach, H. *Surf. Sci.* **1984**, *148*, 292.

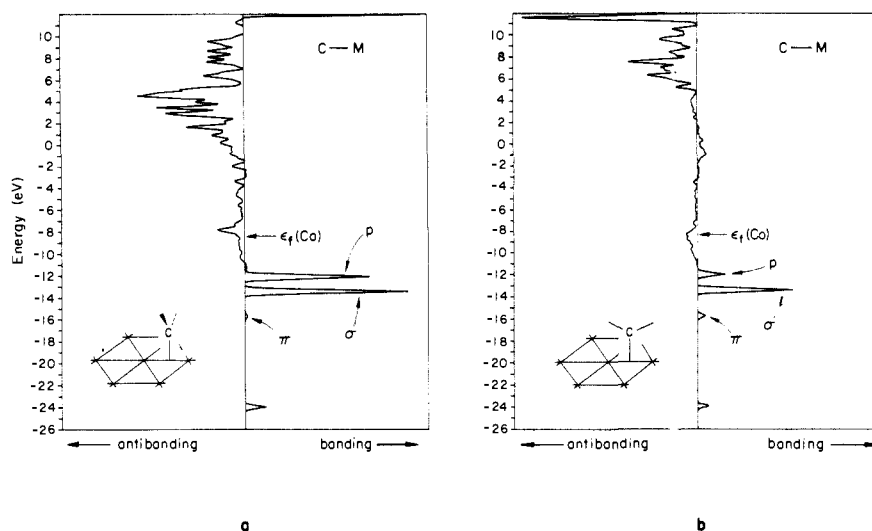


Figure 13. COOP curves for the M-C bond: (a) perpendicular; (b) parallel CH<sub>2</sub> on Co(0001).

result may seem to be in conflict with that for methylene, in fact it is not. Examination of both systems reveals that exactly the same orbitals and interactions dictate the higher stabilities of **56** and **62** relative to the corresponding 90°-rotated structures. The reversed final geometrical outcome results from the different topologies of the orbitals of the two carbenes at hand. In CH<sub>2</sub> the carbene acceptor p orbital is perpendicular to the HCH plane while in vinylidene it lies in the molecular plane. Thus, interactions with the carbene's p orbital dictate a planar geometry **62** for the vinylidene and a perpendicular geometry **56** for methylene. Note that essentially the same reasons lead us to construct the planar ethylene molecule from vinylidene and hydrogens but a tetrahedral (i.e., "perpendicular") molecule (methane) from methylene and H<sub>2</sub>.

An important result of the calculations is that the adsorption of the methylene fragment on all metal surfaces examined has essentially the same energy in the 2-fold perpendicular geometry **56** and in the 1-fold on-top geometry **40**. This result is to be contrasted with methyl adsorption where the 1-fold site (**6**) of Co, Cr, and Ti is preferred over the 2-fold bridged site (**7**) by 1.1, 0.9, and 0.5 eV, respectively. Why do methyl and methylene choose different adsorption sites? The answer lies again in the presence of the empty p orbital of methylene. We have emphasized above for methyl that as the organic fragment moves to a more highly coordinated site its interaction with the surface strengthens, pushing many d states to higher energies. The overall effect is that the total energy rises and the bridged sites become less stable than the 1-fold site. The same effects are operating in the methylene system, but here the additional  $\pi$ -stabilization that is gained in the bridged geometry is so large that it overrides the destabilization that results from the higher energy of the metal-centered bands, and the total energy drops. Indeed, a comparison of the 1-fold site with the bridged parallel position **57** where the  $\pi$ -stabilization is weak reveals the "normal" stability order, with the 1-fold site having the lower energy.

Changing the metal surface has a small effect on the relative energies of the 1-fold and the perpendicular bridged sites. For Co, Cr, and Ti, the energy differences are 0.02, 0.11, and 0.02 eV, respectively, favoring **56**. Similarly, on a Pt surface, vinylidene favors the 2-fold bridged site.<sup>21</sup> These results are also in agreement with those of Minot and co-workers.<sup>18a</sup>

Finally, we comment on the charge distribution. We remind the reader that in analyzing the charges it is useful to look at the separated molecules as [metal]<sup>+</sup> and [organic fragment]<sup>-</sup>. In the case of methylene the charge-transferred extreme is actually CH<sub>2</sub><sup>2-</sup>, p orbital completely filled. As the metal-adsorbent interactions become more efficient electrons are transferred from the adsorbent to the metal. The calculational results for methylene (see Table IV) are very similar to those obtained in the methyl system (see **34** and **35**). In both systems bridging increases the

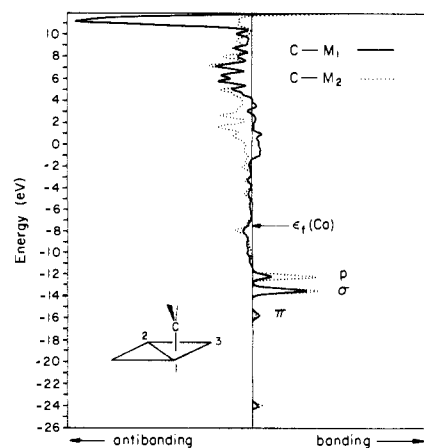


Figure 14. COOP curves for the M1-C and M2-C bonds. The CH<sub>2</sub> group is above the triangular hollow of the Co(0001) surface.



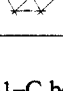
interactions between the metal and the organic fragment and consequently charge is transferred from the adsorbent back to the metal. For example, the charge on the methylene drops from -1.54 to -1.37 when the geometry is changed from the on-top to the 2-fold parallel on the Co surface. More interestingly, the migration of the organic fragment from a 1-fold to a 2-fold site is accompanied by a massive reorganization of charge within the metal slab; electrons flow from the surface layer into the inner layers, avoiding the high-lying bands that are centered around the adsorbing metal atoms. It is instructive that quantitatively these inner metal charge reorganizations are practically identical for the geometry changes **40** → **57** (Table IV) and **6** → **7** (see **34** and **35**). This emphasizes that similar basic changes occur in the metal-adsorbent interactions when the organic fragment migrates from a 1-fold to a 2-fold site, regardless of whether it is methyl or methylene. On top of these basic changes additional interactions, specific to the organic molecule at hand, may alter somewhat the final picture. Thus when the methylene is rotated to geometry **56** and strong  $\pi$  interactions are put into play, additional charge (relative to **57**) flows from the methylene, which becomes less negative, into the metal slab. There it is partitioned mainly between the surface and the B layers.

#### The Threefold Bridging or Capping Geometry, **42**

The analysis of the bonding at this site is straightforward, using the experience gained in the study of the methyl system and of the various adsorption sites of methylene. The COOP curves of the Co-C bonds are displayed in Figure 14. The numbering of the metal atoms and the precise orientation of the methylene group are shown in **63**. The solid line in Figure 14 gives the COOP curve



Table V. Binding Energies and Mulliken Populations of CH Chemisorbed on Various Metal Surfaces

geometry	Fermi level	binding energy (eV)		overlap population			
		$E_1$	$E_2$	$M_1-M_2$	$M_1-C$	M-H	C-H
	Ti	-6.50	15.51	0.95	0.27	0.70	0.79
	Cr	-7.64	11.56	0.30	0.38	0.59	0.78
	Co	-8.53	8.84	0.15	0.17	0.42	0.77
	Ti	-6.49	15.97	1.41	0.13	0.52	0.80
	Cr	-7.58	11.99	0.74	0.22	0.49	-0.02
	Co	-8.51	9.05	0.36	0.09	0.40	-0.01
	Ti	-6.47	16.11	1.55	0.14	0.45	-0.04
	Cr	-7.46	12.43	1.17	0.26	0.43	-0.02
	Co	-8.50	9.36	0.68	0.09	0.39	-0.01

for the Co1-C bond and the dotted line shows the corresponding curve for the two identical Co2-C and Co3-C bonds. The COOP curve shows that, similarly to the 2-fold **56** system, also in **63** both  $\sigma$  (band at -13.6 eV) and  $\pi$  interactions (band at -12.2 eV) contribute effectively to Co-C bonding. Typical  $\sigma$  and  $\pi$  interactions with the metal's  $d_{z^2}$  band are depicted in **64** and **65**, respectively. Similar interactions with other metal bands, in particular s and to some extent  $d_{xz}$  and  $d_{yz}$ , also contribute to bonding.

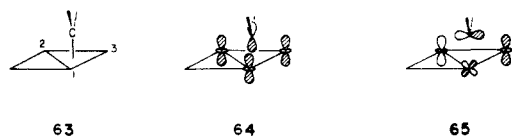


Figure 14 reveals an interesting aspect of the bonding at the 3-fold site and provides a nice demonstration of the analytical power of COOP curves in general.  $\sigma$  bonding (peak at -13.6 eV) is contributed equally (except for a small perturbation induced by the nonsymmetrical arrangement of the methylene hydrogens) by all three metal atoms. In contrast Co2 and Co3 contribute to  $\pi$  bonding (peak at -12.2 eV) much more than Co1. This result can be interpreted quite easily. In **63** the p orbital of methylene is aligned parallel to the Co2-Co3 vector allowing strong overlap with the bands centered around these metal atoms. The topology of the interacting orbitals is similar to that in the perpendicular 2-fold geometry. The interaction of Co1 with the p orbital is much smaller; the situation resembles that of Co1 in the parallel 2-fold geometry. Upon rotation of the methylene group by 30° in a clockwise direction Co1 and Co3 change roles; now Co1 and Co2 contribute to  $\pi$  bonding more than Co3. At intermediate rotation angles metal bands combine effectively to maintain the level of  $\pi$  bonding, so that at the triangular hollow site the adsorbed methylene fragment is essentially freely rotating.

We have already indicated in various places along the discussion that when the organic fragment migrates to a more highly bridged site its interactions with the metal strengthen. Geometry **42** is no exception. For all three metal surfaces the total M-C overlap population (Table IV) is higher in the 3-fold geometry (e.g., 0.83 for Co) than in the 2-fold perpendicular geometry (0.79 for Co). Other trends that we have observed for the 7  $\rightarrow$  8 migration of methyl hold also for methylene (Table IV). As most of the energy which is associated with  $\pi$  bonding was already gained in the 2-fold geometry further bridging leads to the "normal" increase in the total energy, or equivalently to a decrease in the binding energy of the organic molecule to the metal. Binding of methylene at the 3-fold site of cobalt is consequently by 0.6 eV less favorable than binding at the 2-fold or at the on-top sites. A similar trend holds for the Cr and the Ti surfaces.

Finally, we note that we are not aware of molecular trinuclear transition-metal carbene complexes that are stable in the 3-fold capping geometry. Polymetallic carbene complexes usually adopt the 2-fold perpendicular geometry.<sup>1a,12</sup>

We can now proceed to analyze the adsorption of the last fragment, a methyne (CH).

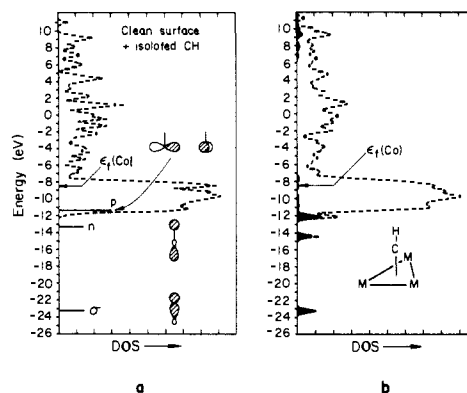
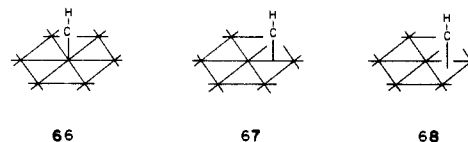


Figure 15. DOS of the CH + Co(0001) slab system before (a) and after (b) CH chemisorbs on the metal surface (capping geometry). CH states are shown by horizontal bars (a) or a darkened area (b).

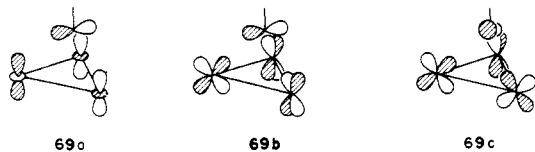
#### Adsorbed Methyne, CH

We will compare three different adsorption sites **66**, **67**, and **68**. Again, the calculations are performed for an "unbiased" C-M distance of 2.1 Å for all three geometries. The binding energies, overlap populations, and charges are tabulated in Table V. We will analyze the bonding based on DOS and COOP curves.



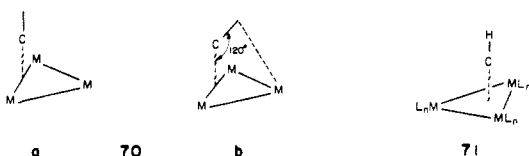
The MOs of the methyne group before and after the adsorption on the hexagonal metal surface in a capping mode are shown in Figure 15. The reason we look at the capping geometry is that this site is the preferred one for both high and low metal electron counts. At the left side are the surface states plus the CH levels before the chemisorption takes place, and the right side is what happens after CH is chemisorbed on the metal surface. CH has five MOs: one of the two carbon sp hybrids pointing toward the hydrogen forms C-H  $\sigma$  and  $\sigma^*$  orbitals. The other hybrid, directed away from the hydrogen, is mainly nonbonding, and so are the degenerate  $p_x$ ,  $p_y$  orbitals. The  $\sigma$  orbital is low in energy and we expect it interacts poorly with the metal d band.  $\sigma^*$  is high up in energy (off-scale in Figure 15), also out of the effective interaction range. What is left for bonding with the surface is the n and  $p_x$ ,  $p_y$  orbitals.

Let us focus on Figure 15b. We see that n is pushed down by  $\sim 1$  eV; at higher energy p is smeared out over the region of -12.3 to -8 eV. Both CH orbitals interact with the metal surface. Which metal orbitals are effective in this interaction? DOS contributions, not shown here, indicate that both metal  $d_{z^2}$  and  $d_{xz}$ ,  $d_{yz}$  are involved. The  $d_{z^2}$  orbital picks up a resonance with the CH p orbital at -12 eV: interactions of type **69a** are important. The  $d_{xz}$ ,  $d_{yz}$  set has resonances with both CH p and  $\sigma$ ; combinations of type **69b** and **69c** are effective.



What happens as CH moves to other adsorption sites, on-top or bridging? We do not show the DOS plots here, but the  $n$  level is pushed down a little less than in the capping site. More of a difference is observed in the fate of the  $p$  level. It is at ca.  $-12.5$  eV for 68,  $-12.1$  eV for 67, and  $-11.7$  eV for the on-top geometry 66.

Motivated by Muetterties and co-worker's suggestion that a CH group might not be perpendicular to the surface due to M-H interaction,<sup>22</sup> we compared two geometries 70a = 67 and 70b. Our calculation shows no significant energetic difference, 70b being slightly higher in energy. Nearly all the organometallic analogues have CH or CR in a symmetrical,  $\mu_3$ , or capping geometry, 71.<sup>32</sup> Binuclear complexes with a bridging CR are well-known,<sup>37a</sup> as are mononuclear  $L_nM\equiv CR$  acetylene analogues.<sup>37b</sup>



To summarize our results concerning various  $CH_x$  groups on the surface, we can simply state that for equal C-M distances, for all adsorption sites, the  $CH_x$  group would prefer to adopt a geometry that can restore its missing C-H bond(s). Thus,  $CH_3$  on-top,  $CH_2$  bridging, and CH capping are energetically the most stable geometries. This agrees with previous theoretical studies and the available experimental information.

So far we have said nothing of reactivity. But most of the experimental studies of  $CH_x$  groups cannot avoid the dynamic aspect. Reactions occur. For example,  $CH_2$  on Fe(100) is believed to dissociate into  $CH + H_2$ , beginning at the bridging position, with one of the C-H bonds parallel to the surface.<sup>33</sup> On a Co surface the dehydrogenation of  $CH_2$  occurs at a relatively low temperature, 180 K, indicating a small barrier for the process  $CH_{2ads} \rightarrow CH_{ads} + H_{ads}$ .<sup>34</sup> In the next section we are going to analyze the migration of  $CH_x$  groups on a surface and how the electronic factor affects various reaction processes.

### Migration on the Surface

Migration of species adsorbed on a surface is a phenomenon of substantial significance in many areas of surface science (e.g., adhesion, lubrication, etc.). For catalysis, the case of interest here, knowledge of the barriers for the migration of the adsorbed fragments is fundamental to the understanding of the mechanism

(32) See, for example: (a) Herrmann, W. A.; Plank, J.; Guggolz, E.; Ziegler, M. L. *Angew. Chem.* **1980**, *92*, 660; *Angew. Chem., Int. Ed. Engl.* **1980**, *19*, 651. Herrmann, W. A.; Plank, J.; Riedel, D.; Ziegler, M. L.; Weidenhammer, K.; Guggolz, E.; Balbach, B. *J. Am. Chem. Soc.* **1981**, *103*, 63. (b) Dimas, P. A.; Duesler, E. N.; Lawson, R. J.; Shapley, J. R. *J. Am. Chem. Soc.* **1980**, *102*, 7787. (c) Howard, M. W.; Kettle, S. F.; Oxtun, J. A.; Powell, D. B.; Sheppard, N.; Skinner, P. *J. Chem. Soc., Faraday Trans. 2* **1981**, *77*, 397.

(33) Rhodin, T. N.; Brucker, C. F.; Anderson, A. B. *J. Phys. Chem.* **1978**, *82*, 894.

(34) Steinbach, F.; Kiss, J.; Krall, R. *Surf. Sci.* **1985**, *157*, 401.

(35) (a) Ertl, G. In *The Nature of the Surface Chemical Bond*; Rhodin, T. N., Ertl, G., Eds.; North-Holland: Amsterdam, 1979; Chapter 5. (b) Schmidt, L. D. In *Interaction on Metal Surfaces*; Gomer, R., Ed.; Springer: Berlin, 1975. (c) Muetterties, E. L.; Rhodin, T. N.; Band, E.; Brucker, C. F.; Pretzer, W. R. *Chem. Rev.* **1979**, *79*, 91.

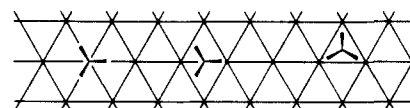
(36) (a) Baetzold, R. *Surf. Sci.* **1985**, *150*, 193. (b) Muetterties, E. L.; Shustorovich, E.; Baetzold, R. C., preprint. (c) Shustorovich first treated the migration barrier in a chemical way: Shustorovich, E. *J. Am. Chem. Soc.* **1984**, *106*, 6479. (d) For an excellent review see: Shustorovich, E. *Surf. Sci. Rep.* **1986**, *6*, 1. (e) A recent theoretical study suggests that for  $CH_3$  on Ni, Pd, and Pt(111) the on-top site is less stable by 4 kcal/mol than the bridging site: Shustorovich, E. *Surf. Sci.* **1986**, *176*, L863.

(37) (a) Holton, J.; Lappert, M. F.; Pearce, R.; Yarrow, P. I. *W. Chem. Rev.* **1983**, *83*, 135. (b) Fischer, E. O.; Shubert, U. *J. Organomet. Chem.* **1975**, *100*, 59.

of surface reactions. In the FT synthesis, for example, it is important to know if in the coupling step (step 3, Scheme I) the rate-determining process is the migration of the two (or more) fragments toward each other or if it is the chemical barrier associated with the coupling reaction itself. Unfortunately, the experimental characterization of surface migration (or diffusion) is difficult,<sup>35</sup> and for the  $CH_x$  fragments little such information is available.

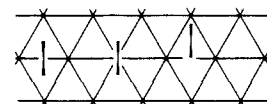
Recently, Muetterties, Shustorovich, and Baetzold developed a remarkably useful and versatile theoretical model for surface migration of atoms and diatomic molecules.<sup>36</sup> This is based on a Morse potential for the metal-adsorbent interaction and on the assumption that the M-X (M = metal, X = adsorbent) bond order is conserved along the migration path.<sup>36</sup> Our approach is different and is based on the actual calculation of several selected points on the potential energy surface. All necessary data for analyzing the migration of the  $CH_x$  fragments on the metal surface already have been presented above. A disadvantage of our approach already has been mentioned above—we rely on a molecular orbital method that is very approximate, especially when it deals with the energetics of bond formation. The conclusions we reach gain a little strength when they are supported by overlap population analysis, which together with the energies and other bonding arguments form a self-consistent conceptual picture.

In drawings 72, 73, and 74 we have collected what the computations give for the relative binding energies (in eV) at the three symmetry distinguished adsorption sites of methyl, methylene, and methyne, respectively. In each drawing we present the calculated values for Co, Cr, and Ti surfaces.



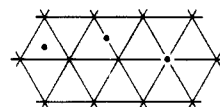
Relative E (eV):			
Co :	0.0	1.1	1.4
Cr :	0.0	0.9	0.9
Ti :	0.0	0.5	0.1

72



Relative E (eV):			
Co :	0.0	0.0	0.6
Cr :	0.0	0.1	0.5
Ti :	0.0	0.0	0.3

73



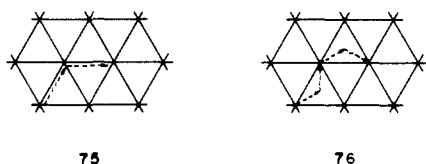
Relative E (eV):			
Co :	0.0	0.3	0.5
Cr :	0.0	0.4	0.9
Ti :	0.0	0.1	0.6

74

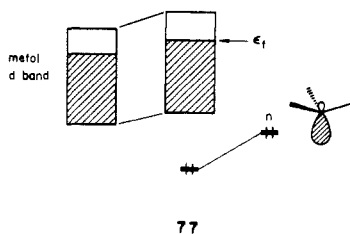
A low migration barrier can be observed only if there are at least two sites connected or nearby on the metal surface for which the binding energies of the organic fragment are similar. Let us call these sites A and B. In this case the lowest energy path for the migration of the fragment is simply along the  $A \rightarrow B \rightarrow A \dots$  path. The energy barrier for the migration is then determined by the energy differences between points A and B. The relative energies of other binding sites (C, D, etc.) are of no significance to the migration process because even if these points are very high

in energy they can be circumvented by migration along the A → B → A path.

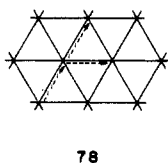
Let us look first at the migration of a methyl fragment that is shown in 72. For a cobalt surface the site with the highest binding energy (i.e., the lowest point on the potential energy surface) is the 1-fold "on-top" site. The two other sites are considerably higher in energy. The lower energy one of these is the 2-fold site, 1.1 eV higher in energy than the 1-fold site. The theoretical prediction is that the migration of methyl on a cobalt surface will require relatively high temperatures and should proceed mainly along the (formal) metal-metal bonds, via the path shown by the dotted line in 75. Migration occurs along the (formal) metal-metal bonds. When the electron count on the metal is lowered the bridged positions are differentially stabilized and the barriers to migration should be considerably lower. For the Ti surface the barrier to migration along the path shown in 76 (which is the lowest in energy) is only 0.1 eV. For the Cr surface the barrier is calculated to be the same (0.9 eV) along either path 75 or 76.



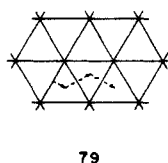
Why does the migration barrier decrease as the metal d band is depopulated? Remember the main interaction is between the methyl lone pair *n* and the metal d band, 77. The metal d band region is weakly C-M antibonding (cf. Figure 4). The strength of the antibonding character depends on the overlap between *n* and the metal d band. The higher the coordination number of the CH<sub>3</sub> group, the stronger the C-M antibonding character in the metal d band. Thus at high d band filling the capping geometry is less stable, because of its stronger C-M antibonding contribution within the increasingly occupied d band. At lower band filling the C-M antibonding feature is reduced, and the higher coordination sites of CH<sub>3</sub> stabilize *n* more. So the barrier is reduced.



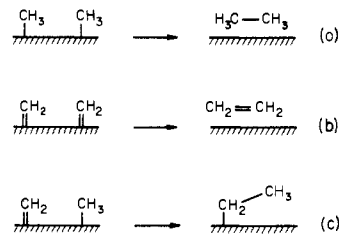
For methylene the situation is different. Migration on a cobalt surface occurs with no barrier along a path (with no rotation of the CH<sub>2</sub> group) shown by the dashed line in 78. The same lowest energy migration path is calculated for CH<sub>2</sub> on the Cr and Ti surfaces (see also the more detailed discussion above).



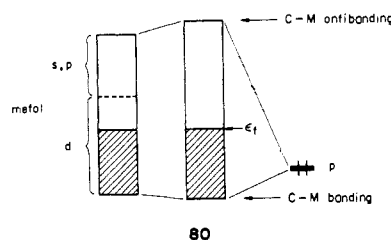
The migration of a CH fragment is relatively facile; the barriers along path 79 are only 0.3, 0.4, and 0.1 eV for Co, Cr, and Ti, respectively. This migration path remains the lowest in energy for all metals, and for those with lower electron counts the binding preference for the 2- and 3-fold sites even increases.



## Scheme III



The reason that the migration barriers for CH<sub>2</sub> and CH do not change much at low metal band filling derives from the fact that in addition to orbital *n* ( $\sigma$ ) some other orbitals (*p*) also play a decisive role in the bonding. Details of the analysis have been given above. One can say that the *p* orbital, being very close to the *d* band in energy, mixes very strongly with the metal orbitals (cf. Figures 10 and 12). This mixing, shown in 80, may contribute to C-M bonding even at high *d* band filling. Thus two types of interaction, 77 and 80, compete to determine the migration barrier.



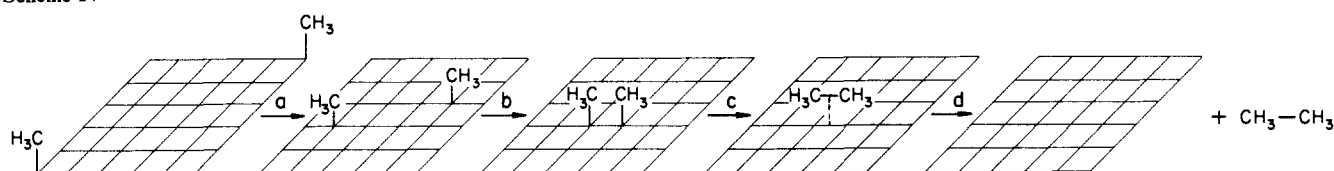
Knowledge of the barriers to migration has, of course, interesting implications regarding the coupling steps in the FT synthesis. For example, the calculations suggest that on a cobalt surface, the coupling of methyl and methylene may occur preferably by migration of CH<sub>2</sub> toward the adsorbed methyl rather than by migration of methyl. Furthermore, the coupling of two methyl fragments may involve a substantial barrier for migration, while the coupling of two methylenes should require no such barrier. To demonstrate the implications of these results let us assume that the barriers to the coupling processes themselves are small so that the migration processes determine the rate of the FT reaction. The above results suggest that in such a case the rate of coupling of two methyls, but not that of two methylenes, should be reduced at lower temperatures. Thus, the coupling of two methylenes (or of a methylene and a methyl) would be favored at lower temperatures and higher yields of ethylene expected. Similar analysis can lead to interesting conclusions regarding the Cr and Ti metal surfaces and the other coupling reactions.

## The Coupling Reactions

The coupling reactions in Scheme III model some of the processes that determine chain length and olefin proportion among the FT product. In this treatment we assume that methyl and methylene are reasonably good models for other adsorbed alkyl (C<sub>n</sub>H<sub>2n+1</sub>) or alkylidene (C<sub>n</sub>H<sub>2n</sub>) fragments. Thus, the coupling of two methyls (reaction a in Scheme III) models a termination step that yields alkanes. A similar termination process (not shown here), that also yields alkanes, is the coupling of adsorbed alkyl and H fragments. A termination process, leading to olefins, is modeled by the coupling of two methylenes (reaction b in Scheme III). The coupling of methylene and methyl (reaction c in Scheme III) models the major propagation step in the FT reaction. Other coupling reactions that may also contribute to the overall FT process, e.g., CH<sub>2</sub> + CH → CH<sub>2</sub>=CH, were not included in this study.

By studying these coupling processes we hope to gain understanding into basic questions concerning the FT synthesis. Typical questions are the following: What are the factors that control these reactions? Are steric or electronic factors more important? Why does the Schult-Flory distribution change when the metal catalyst is varied?<sup>1c</sup> We cannot answer these questions definitely, but we hope to extract some useful information from our calcu-

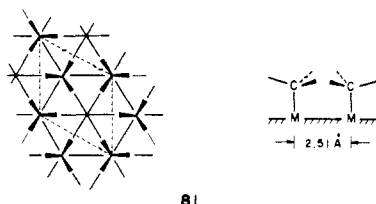
Scheme IV



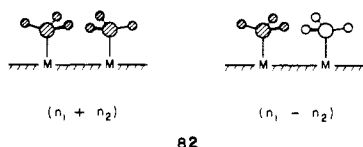
lations. Insight into these problems, even at a relatively primitive level, could help chemists design new catalysts with improved selectivities.<sup>52</sup>

We find it conceptually advantageous to partition each coupling reaction and the energy barrier associated with it into four discrete steps, shown schematically in Scheme IV. The first is the migration process (step a in Scheme IV), which was discussed in detail in the previous section. In the second step the reacting fragments reach two adjacent metal atoms (step b in Scheme IV). The energy that is associated with this step is denoted as the "proximity" energy (PE), and it is not directly related to the migration barrier. The migration barrier is the lowest energy that is required for the migration of a fragment from one binding site to the other, with no other fragments in close proximity, i.e., at near zero coverage. The "proximity" energy denotes the energy that is required (or which is liberated) to bring the fragments to neighboring binding sites. The PE gives information on the interactions (steric and electronic) between the reactant fragments at early stages of the coupling process. It is also obviously related to the energetics of moving from low to high coverage. The third step (step c in Scheme IV) is the coupling reaction itself. The last step (d in Scheme IV) corresponds to desorption removal of the product molecule from the surface. One would not expect any activation energy for desorption of ethane, so steps c and d will merge in that case. But if the product is unsaturated—an alkyl group or an ethylene—it might stick to the surface after coupling. The total energy that is required to execute a certain reaction is affected by the energies of these 4 steps, i.e., migration, "proximity", coupling, and desorption.

Let us proceed now to discuss these discrete steps for the reactions in Scheme III. First a technical note on the way the calculations were carried out. All the previous calculations, for reasons of computational economy, were performed assuming a 1/3 coverage. If we bring another CH<sub>3</sub> group into the unit cell, the high 2/3 coverage will certainly lead to great crowding. A geometry such as **81** is forced. In our calculation for this and all other reactions we delete the interactions of the C<sub>1</sub> groups between unit cells, so that there is no crowding whose cause is *inter-cell* interaction. In other words, we are modeling a reaction in which two methyl groups come together locally, but remain isolated from other methyls on the surface. On the Cr surface the C<sub>1</sub> fragments were attached to metals along the shorter Cr–Cr bonds of 2.49 Å.



**The "Proximity" Energies (PEs).** The DOS curves for CH<sub>3</sub> on Co in such a coverage (not shown here) show a splitting of all CH<sub>3</sub> states. Such a splitting in the occupied states, shown in **82** for a low-lying  $\sigma$  orbital, is highly destabilizing as it is a typical four-electron two-center repulsion. The COOP curves also indicate regions of C–C antibonding.



**83** gives computed binding energies per CH<sub>3</sub> for the coverage shown in **81** but with all *inter-cell* interactions cut. For comparison, **83** also gives binding energies of an "isolated" adsorbed CH<sub>3</sub> fragment (see Table III). The differences between these binding energies, also presented in **83**, give the "proximity" energies (PEs) per CH<sub>3</sub> fragment. In the indicated eclipsed geometry the calculated methyl PEs (per CH<sub>3</sub> fragment) are 0.7, 0.5, –0.1 eV for the Co, Cr, and Ti surfaces, respectively. The energies required to bring two methyl fragments to neighboring surface metal atoms are twice the above values.


Binding E per CH <sub>3</sub> (eV) :			
	"isolated"	BE	PE
Ti	5.4	5.5	-0.1
Cr	4.3	3.8	0.5
Co	3.7	3.0	0.7

**83**

To gain additional information on the origin of the "proximity" energies we have compared the above PEs with the corresponding values for the two "nonbound" eclipsed methyl groups (i.e., omitting the metal surface in **83**). The energy of two "nonbound" eclipsed methyl radicals which are separated by a C–C distance of 2.51 Å (as in **83**) is 1.2 eV higher than that of two isolated non-interacting methyl fragments. This value reflects the strong steric repulsions between the hydrogens which are only 1.48 Å apart. Rotation of one of the methyl groups by 60° to a staggered conformation increases the steric congestion even further and the repulsion energy rises to 2.7 eV. The steric interactions are reduced considerably (i.e., to only 0.2 eV in the eclipsed conformation), at a separation of 2.95 Å—the M–M distance in the Ti surface. The adsorbed organic fragments are negatively charged (Table III) so that it is reasonable to assume that the interaction between two "nonbound" methyl anions is a better model for the surface situation than the interaction between two neutral methyl radicals. At C–C separation distances of 2.51 and 2.95 Å the repulsion between two "nonbound" eclipsed methyl anions is 1.8 and 0.4 eV, respectively. Indeed, on the Co surface the PE of two adsorbed CH<sub>3</sub> groups is 2 × 0.7 = 1.4 eV, a value intermediate between the interaction energies of two "nonbound" CH<sub>3</sub> radicals and anions. This value is of reasonable magnitude considering that the charge on the adsorbed methyl is –0.59 (Table III). However, the steric and electrostatic repulsion between the negatively charged alkyl groups do not reveal the entire story. For example, on the Cr surface, two adsorbed CH<sub>3</sub> groups repel each other by 1.0 eV, although at the same separation distance (2.49 Å) the repulsion between two "nonbound" methyl groups, either neutral or negatively charged, is much larger (2.8 eV for the radicals). Similarly, on the Ti surface the negatively charged (–0.79) adsorbed methyl groups attract each other by 0.2 eV, while at the same C–C separation the interaction between two "nonbound" methyl fragments, either neutral or negatively charged, is repulsive. Apparently, as the two adsorbed methyls approach each other additional *attractive* forces come into action. We have not identified the electronic origin of these attractive forces in detail, but we note that their magnitude depends on the metal and that they are relatively small for Co and larger for Cr and Ti. The electronic nature of these attractive forces can be demonstrated also in the following manner. When the calculations for the Ti surface are repeated with use of the shorter Co–Co distances of 2.51 Å, the PE for CH<sub>3</sub> increases moderately, from –0.1 to 0.3 eV. However, this value is still significantly lower than

the methyl PE on cobalt of 0.7 eV, although the methyl groups are more negatively charged when adsorbed on Ti (Table III). Apparently, for the Ti surface there is an additional attractive electronic effect (compared to Co) which compensates for the increased electrostatic repulsions between the methyls at the shorter M-M distance of 2.51 Å. Calculations for the Ti surface with use of the "rigid band" model (i.e., with the Co EH parameters and surface geometry, but a  $d^4$  occupancy) give a PE of 0.8 eV, much higher than the 0.3 eV calculated with use of the same geometry but with the Ti parameters. This suggests that the position of the Fermi level, rather than the  $d$  occupancy, plays the dominant role in determining these PEs.

The calculated PEs for methylene groups (per  $CH_2$ ) are given in 84. As with the methyls, the PE decreases from Co to Cr and it becomes attractive for Ti. The absolute values of the PE are generally somewhat smaller for  $CH_2$  than for  $CH_3$ .

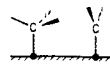


Binding	E per $CH_2$ (eV)	$E_1$	
		"isolated"	BE PE
Ti	10.4	10.5	-0.1
Cr	8.0	7.7	0.3
Co	6.3	5.8	0.5

84

The PEs in 84 can be compared with the analogous values for two "nonbound"  $CH_2$  groups. At a C-C distance of 2.51 and 2.95 Å two neutral methylenes attract each other by 0.7 and 0.1 eV, respectively, while two doubly negatively charged  $CH_2$  groups repel each other by 1.3 and 0.3 eV, respectively. These energies should be compared with the PEs in 84 multiplied by 2. The adsorbed  $CH_2$  groups are strongly charged (-1.54, -1.53, and -1.59 on the Co, Cr, and the Ti surfaces, respectively, Table IV), and their mutual electrostatic repulsion is the major factor that determines the PE in 84. Steric effects are unimportant. As for the  $CH_3$  groups, also with the  $CH_2$  fragments, a compensating attractive force reduces the PEs so that they are smaller than expected on the basis of the electrostatic repulsions alone.

The PEs for neighboring methyl and methylene fragments are given in 85 (the given values are for the two fragments). The geometry of the organic fragments in 85 is electrostatically the most stable arrangement. At a C-C separation of 2.51 Å rotation of the methyl group by  $60^\circ$  has almost no effect on the energy of "nonbound"  $CH_3 + CH_2$  fragments, but the energy increases by 1 eV for the triply charged ( $CH_3 + CH_2$ ) unit. Similarly, on Co a  $60^\circ$  rotation of the methyl group increases the PE from 1.2 to 2.4 eV. The ( $CH_3 + CH_2$ ) PEs in 85 can be understood as being simply the sum of the PEs of  $CH_3$  and of  $CH_2$ . For example, on Co,  $PE(CH_3) + PE(CH_2) = 0.73 \text{ eV} + 0.53 \text{ eV} = 1.26 \text{ eV}$ , compared with the directly calculated  $PE(CH_3 + CH_2)$  of 1.21 eV (see 85). Thus, the electronic and steric effects discussed above for  $CH_3$  and  $CH_2$  dictate also the PEs for the  $CH_3 + CH_2$  couple. Let us proceed to analyze the coupling processes in Scheme III.



Binding	E (eV)	$E_1$	
		"isolated"	BE PE
Ti	15.8	16.0	-0.2
Cr	12.3	11.5	0.8
Co	10.1	8.8	1.2

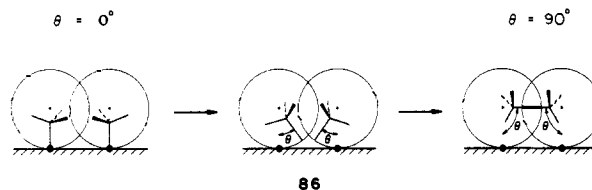
85

**The Coupling Reactions.**  $CH_3 + CH_3$ . What happens when two  $CH_3$  groups couple? First, let us examine the overall thermodynamics of the process. In the coupling process a new C-C bond is formed but two M-C bonds are lost. Whether the reaction is exothermic or endothermic is determined primarily by the relative strengths of these bonds (the surface binding energy of ethane is assumed to be much smaller than the above bond energies), which are not easily obtainable experimentally and which

cannot be calculated reliably with the extended Hückel method. However, we believe that the calculations are sufficiently reliable to allow us to comment on the changes that occur in the reaction thermodynamics as the metal surface is changed. Thus, as the metal is changed from Co to Ti the M-C bond energy increases (see binding energies in 83 or Table III) and this should increase the endothermicity of the coupling reaction, as is indeed found in the calculations (see below). Thus, the coupling of two methyl groups becomes increasingly endothermic, i.e., by 0.9, 4.7, and 7.1 eV, on moving along the series  $Co \rightarrow Cr \rightarrow Ti$ , respectively.

What can we predict for the barrier to the dimerization reaction? Here interesting electronic factors, *specific to reactions occurring on metal surfaces, come into action*. The reaction begins with both  $CH_3$  lone pairs nearly filled, i.e., near a  $CH_3^-$  representation. As the reaction proceeds a new C-C  $\sigma$  bond forms, and as usual we must consider  $\sigma$  and  $\sigma^*$  combinations, i.e.,  $n_1 \pm n_2$ . Both are filled initially, but as the C-C bond is more completely formed the  $\sigma^*$  ( $n_1 - n_2$ ) combination will be pushed up in energy and eventually will dump its electrons into the metal  $d$  band.

Let us sample such a reaction on the surface by using a transit along a single reaction coordinate  $\theta$ , see 86. The "umbrella handle" of the  $CH_3$  group is moved along and perpendicular to an arc of a circle. The circle is defined as "standing" on the metal atom, such that when the rotation angle  $\theta = 90^\circ$  the C-C distance is 1.54 Å as in ethane (C to surface separation is 2.59 Å).  $\theta = 0^\circ$  corresponds to the initial geometry with the "umbrella handle" perpendicular to the surface and bonded to the metal atom, M-C being 2.1 Å. This transit is probably not optimal, a true reaction path, but it can give us some information concerning the controlling electronic factors. Unfortunately, full exploration of the potential surface is not realistic with our computational capabilities and method.



86

Figures 16 and 17 show the methyl lone pair contribution to the total DOS and C-C COOP curve along the reaction coordinate  $\theta$ . Before the coupling starts ( $\theta = 0^\circ$ )  $n-CH_3$  already has split into two peaks around -13 eV. The higher one is  $n_1 - n_2$  and the lower one  $n_1 + n_2$  (cf. 82). But at a C-C separation of 2.51 Å and with the two "umbrella handles" parallel,  $n_1 - n_2$  is still hardly antibonding. At  $\theta = 30^\circ$  the antibonding portion (-12 to 7 eV, of Figures 16 and 17) separates from the bonding part (-14 eV) and at  $\theta = 60^\circ$  it is well above the Fermi level.

What if the position of the Fermi level changes? From the above discussion the total energy of the system increases along the path as  $n_1 - n_2$  becomes more antibonding. When  $n_1 - n_2$  is pushed above the Fermi level it becomes empty. After this turning point in the reaction path the total energy should go down again as  $n_1 + n_2$  becomes continuously more bonding. *The position of the Fermi level determines the turning point and the barrier height. The higher the Fermi level, the further away that turning point is from the starting geometry (i.e., a "late" or "product-like" transition state), and the higher the barrier.* Figure 18, showing the computed energy profile along the idealized reaction path, confirms this line of reasoning. The coupling barrier on Co is lower than that on Cr, which in turn is lower than that on Ti. Note that the "proximity" energies (see 83) decrease as the metal is changed from Co to Cr to Ti, while the actual coupling barriers and the reaction endothermicities increase from Co to Ti. Thus, the "proximity" energies act to moderate the differences in the coupling energies between the different metals. (As with other extended Hückel energies, we do not trust the absolute energies sufficiently to try to predict the actual coupling barriers.)

We note here some important connections to earlier work: Mango and Schachtschneider made a clever suggestion early on

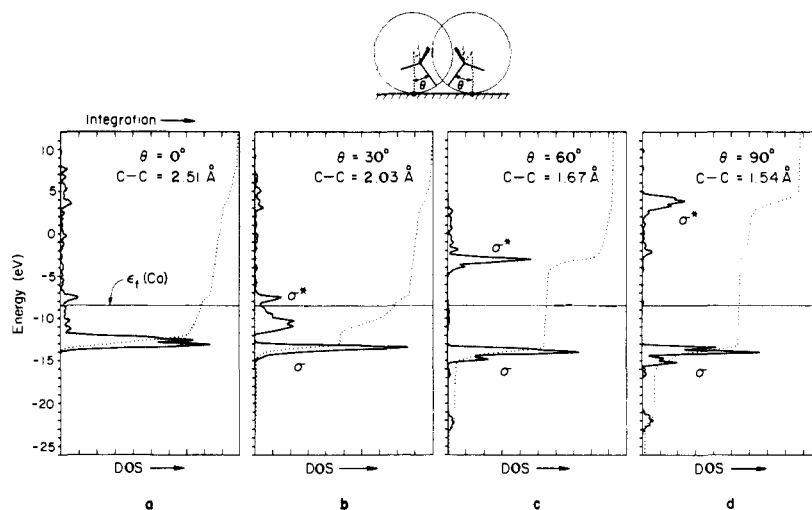


Figure 16.  $n\text{-CH}_3$  DOS evolution in the coupling reaction of two  $\text{CH}_3$  fragments on  $\text{Co}(0001)$ . The reaction coordinate  $\theta$  is defined in 86.

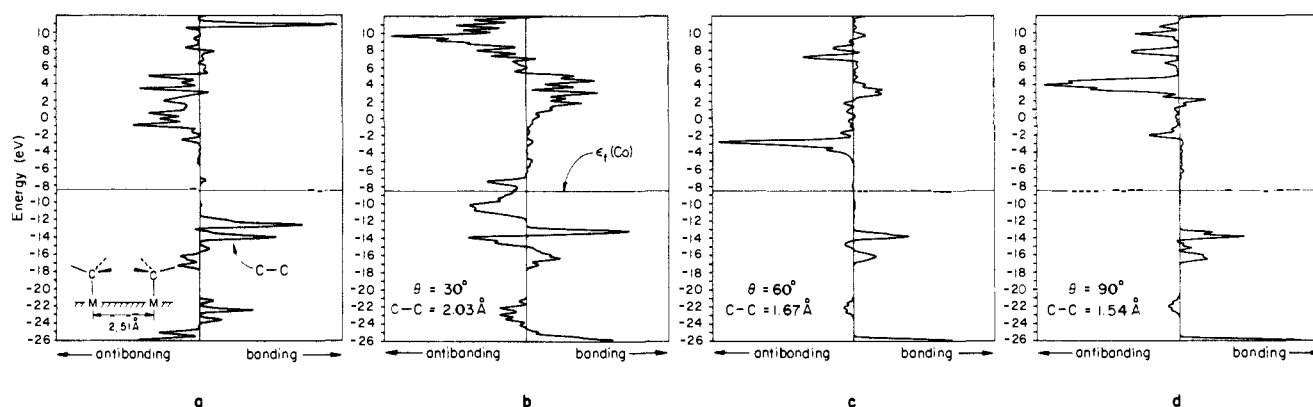


Figure 17. C-C COOP evolution in the coupling reaction of two  $\text{CH}_3$  fragments on  $\text{Co}(0001)$ , as a function of the reaction coordinate  $\theta$ .

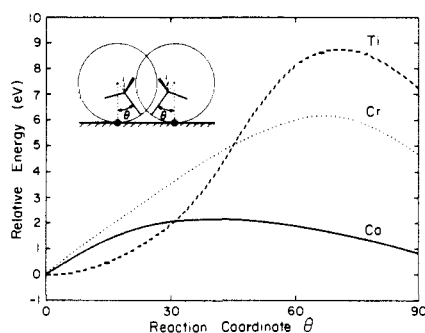
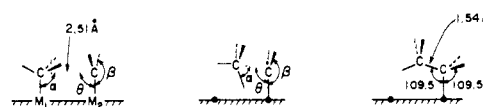


Figure 18. Relative energy of the  $\text{CH}_3 + \text{CH}_3$  system along the coupling reaction path  $\theta$ . The three curves correspond to different metal surfaces (Co, Cr, and Ti).

on the way in which metal atoms (with associated ligands) lower the activation barriers for forbidden concerted reactions.<sup>38b</sup> They pointed out that such electrons, instead of proceeding on to high antibonding levels, can be transferred to the metal. We, and others, have worked out the details of this kind of catalysis for some specific organometallic reactions, such as reductive elimination.<sup>38b</sup> Lichtenberger and co-workers have cleverly used photoelectron spectroscopy to guide a similar line of thought about coupling reactions.<sup>38c</sup> We ourselves have studied the coupling of

methylenes and methynes on mono- and dinuclear complexes.<sup>38d</sup>

**$\text{CH}_3 + \text{CH}_2$ .** This reaction models the chain propagating step in the FT process. The reaction coordinate is chosen to be a single parameter  $\theta$ , see 87. Along the reaction path the C-C distance (decreasing from 2.51 to 1.54 Å), the angle  $\alpha$  between the C-C bond and the  $\text{CH}_3$  "umbrella handle" (also decreasing, from  $90^\circ$  to  $0^\circ$ ), and the HCM2 angle  $\beta$  on the  $\text{CH}_2$  group (decreasing from  $120^\circ$  to  $109.5^\circ$ ) are chosen to vary linearly with  $\theta$ .  $\theta$  itself changes from  $90^\circ$  to  $109.5^\circ$ .



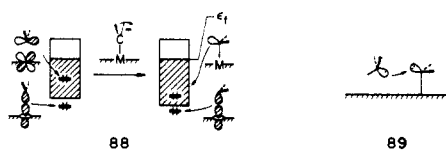
87

Also here we can make some predictions about the thermodynamics of the coupling reaction. Assuming that the binding energies of  $\text{CH}_3$  and of  $\text{CH}_2\text{CH}_3$  are similar, the coupling of  $\text{CH}_3$  and  $\text{CH}_2$  can be analyzed as involving the formation of a C-C bond and the loss of a formal  $\text{M}=\text{CH}_2$  double bond. As the binding energy of  $\text{CH}_2$  increases on going from Co to Ti (Table IV or 84) it is expected and indeed found computationally that the endothermicity of the coupling reaction decreases along the series  $\text{Ti} \rightarrow \text{Cr} \rightarrow \text{Co}$ .

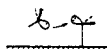
Let us look now on the reaction barrier. The  $\text{CH}_2$  group, formally bonded to the surface by a double bond, loses some of its C-M bonding when the hydrogens are bent downwards. This is because the  $\text{CH}_2$  orbitals rehybridize and in the final geometry there is a hybrid pointing away from the metal atom, shown in 88. That hybrid is gradually pushed up by an approaching methyl n orbital, 89. Thus, the potential energy curve should rise due to the four-electron repulsion 88, and then drop down after the

(38) (a) Mango, F. D.; Schachtschneider, J. H. *J. Am. Chem. Soc.* **1967**, *89*, 2848. Mango, F. D. *Coord. Chem. Rev.* **1978**, *15*, 109. (b) Hoffmann, R. In *IUPAC. Frontiers of Chemistry*; Laidler, K. J., Ed.; Pergamon: Oxford 1982. Tatsumi, K.; Hoffmann, R.; Yamamoto, A.; Stille, J. K. *Bull. Chem. Soc. Jpn.* **1981**, *54*, 1857 and references therein. (c) Lichtenberger, D. L.; Kellogg, G. E. *Acc. Chem. Res.* **1987**, *20*, 379 and references therein. (d) Wilker, C. N.; Hoffmann, R.; Eisenstein, O. *Nouv. J. Chim.* **1983**, *7*, 535.

antibonding level is pushed above the Fermi level and transfers its electrons to the metal.



88

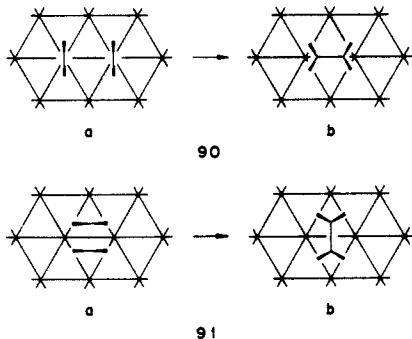


89

The contribution of the methylene p orbital to the total DOS along the reaction coordinate (not shown here) is similar to that of the methyl n orbital in Figure 16. A portion of the total contribution, corresponding to the C-C  $\sigma^*$  level, gradually climbs from below the Fermi level. The computed potential energy curve along the reaction path also has the same feature as that in Figure 18 for the methyl coupling case. Again for reasons similar to those discussed for the  $CH_3 + CH_3$  case, as the metal Fermi level is lowered the barrier height is reduced and the activation energy peak is shifted to the left side, i.e., to a more "reactant-like" transition state. The n- $CH_3$  and  $\sigma$ - $CH_2$  (=n- $CH_2$ ) states also have as expected a portion corresponding to the C-C  $\sigma^*$  level rising up along the reaction path, but these graphs are not shown here.

We should like to mention here the recent remarkable demonstration of methyl-methylene coupling in model binuclear organometallic systems by Maitlis and co-workers.<sup>12d</sup>

$CH_2 + CH_2$ . The surface precursor could start in either a parallel, **90**, or a perpendicular geometry, **91**. The possibility of the perpendicular mode is anticipated from our earlier discussion that on the hexagonal surface the capping geometry for a  $CH_2$  group may have lower energy for low d band filling (see **73** and **80**). However, geometry **91a**, with each  $CH_2$  group sitting directly above the metal triangular hollow, requires a C-C separation of 1.45 Å. This is obviously not a realistic starting geometry and our calculation indeed gives a large repulsion for **91a**.



90

91

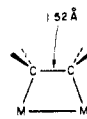
To find the appropriate reaction path for that geometry is beyond our means. Instead we will explore some limited parts of the potential surface, in particular those very close to the final product in the coupling process. Before we proceed to analyze in some detail the geometry of the product ethylene we note that calculations similar to those discussed above for reactions a and c in Scheme III (starting from geometry **90a** and using  $\theta$  as the reactions coordinate) suggest that in contrast to the other reactions the coupling of two methylenes is exothermic and that *no energy barrier exists along the reaction path*. Thus, the theoretical prediction for all three metal surfaces is that the coupling of two methylenes is continuously exothermic, so that when two methylenes reach neighboring metal sites they couple spontaneously. This implies that the assembly of the two organic fragments (i.e., the PEs in **84**) is the only endothermic step in the surface coupling of two methylenes. This contrasts with the coupling of two methyls (Figure 18) and of a methyl and a methylene, where the reactions are endothermic and energy barriers exist along the reaction path. There are of course obvious differences in the desorption step that might follow these coupling reactions.

Let us now discuss the geometry of the adsorbed product.

#### Ethylene Adsorbed on a Co Surface

But what is the final geometry? The known molecular complex **92** has a "parallel" geometry. The C-C distance is  $\sim 1.52$  Å,

characteristic of a single bond. The C-M distance is  $\sim 2.0$  Å (M = Fe),<sup>39a</sup> and the hydrogens bend away from the metal.



92

Some information is available concerning the geometry of chemisorbed ethylene. Ibach and Lehwald have compared the vibrational frequencies of  $C_2H_4$  on Pt(111) with those of Zeise's salt ( $[K[PtCl_3(C_2H_4)] \cdot H_2O]$ ) and concluded that the carbon atoms have  $sp^3$  hybridization.<sup>40a</sup> Comparison of experimental photoemission data with an SCF-LCAO calculation on ethylene in different geometries by Demuth suggested that the C-C distance is 1.34–1.49 Å and the C-C-H angle is 106–109.5° for ethylene on Cu(111), Ni(111), Pd(111), and Pt(111).<sup>40b</sup> A recent HREELS study by Stroschio, Bare, and Ho also suggests that adsorbed ethylene is characterized by  $sp^3$  hybridization.<sup>41a</sup> Comparison of NEXAFS of gaseous and chemisorbed (on Pt(111)) ethylene led to a proposal of a single C-C distance of 1.53 Å.<sup>41b</sup>

Interestingly, on Pt(111) precovered with oxygen there is a mixture of both di- $\sigma$ -bonded ( $sp^3$ ) and  $\pi$ -bonded ( $sp^2$ ) ethylene.<sup>42a</sup> On NiO(100) evidence exists for two adsorption states of ethylene.<sup>42b</sup> At high temperature ethylene also transforms into ethylidyne,  $H_3C-C\equiv$ .<sup>42,43</sup> Other possibilities include hydrogenolysis<sup>44</sup> or dehydrogenation<sup>43c</sup> of ethylene on the surface. Since the pioneering work of Rösch and Rhodin,<sup>45d</sup> Anderson,<sup>45e</sup> and Demuth,<sup>40</sup> there have been many theoretical studies of ethylene interacting with metallic clusters of finite size.<sup>45</sup> A recent paper by Baetzold<sup>45f</sup> also studies ethylene on late transition-metal (111) surfaces.

From the available experimental information we choose the following geometry: C-C = 1.45 Å, the HCH plane bent upward

(39) (a) Bonnet, J. J.; Mathieu, R.; Poilblanc, R.; Ibers, J. A. *J. Am. Chem. Soc.* **1979**, *101*, 7487–7496. (b) Green, M.; Laguna, A.; Spencer, J. L.; Stone, F. G. A. *J. Chem. Soc., Dalton Trans.* **1977**, 1010–1016. (c) Motyl, K.; Norton, J. R.; Schauer, C. K.; Anderson, O. P. *J. Am. Chem. Soc.* **1982**, *104*, 7325–7327. (d) Burke, M. R.; Takats, J.; Grevels, F.-W.; Reuvers, J. G. A. *J. Am. Chem. Soc.* **1983**, *105*, 4092–4093. (e) Theopold, K. H.; Bergman, R. G. *Organometallics* **1982**, *1*, 1571–1579. (f) Dedieu, A.; Hoffmann, R. *J. Am. Chem. Soc.* **1978**, *100*, 2074–2079.

(40) (a) Ibach, H.; Lehwald, S. *J. Vac. Sci. Technol.* **1978**, *15*, 407. (b) Demuth, J. E. *IBM J. Res. Dev.* **1978**, *22*, 265.

(41) (a) Stroschio, J. A.; Bare, S. R.; Ho, W. *Surf. Sci.* **1984**, *148*, 499. (b) Stöhr, J.; Sette, F.; Johnson, A. L. *Phys. Rev. Lett.* **1985**, *53*, 1684. (c) Horsley, J. A.; Stöhr, J.; Koestner, R. J. *J. Chem. Phys.* **1985**, *83*, 3146.

(42) (a) Steininger, H.; Ibach, H.; Lehwald, S. *Surf. Sci.* **1982**, *117*, 685. (b) Furstenau, R. P.; Langell, M. A. *Surf. Sci.* **1985**, *159*, 108.

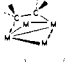
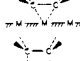
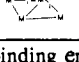
(43) (a) Koestner, R. J.; van Hove, M. A.; Somorjai, G. A. *Surf. Sci.* **1982**, *121*, 321. (b) Lloyd, D. R.; Netzer, F. P. *Ibid.* **1983**, *129*, L249. (c) Creighton, J. R.; White, J. M. *Ibid.* **1983**, *129*, 327. (d) Demuth, J. E. *Ibid.* **1979**, *80*, 315, 367. (e) Albert, M. R.; Snedden, L. G.; Eberhardt, W.; Greuter, F.; Gustafsson, T.; Plummer, E. W. *Ibid.* **1982**, *120*, 19. (f) Baro, A. M.; Ibach, H. *J. Chem. Phys.* **1981**, *74*, 4194. (g) Ibach, H.; Hopster, H.; Sexton, B. *Appl. Phys.* **1977**, *14*, 21. (h) Felner, T. E.; Weinberg, W. H. *Surf. Sci.* **1981**, *103*, 265. (i) Gates, J. A.; Kesmodel, L. L. *Ibid.* **1983**, *124*, 68; **1982**, *120*, L461. (j) Kesmodel, L. L.; Gates, J. A. *Ibid.* **1981**, *111*, L747. (k) Lehwald, S.; Ibach, H. *Ibid.* **1979**, *89*, 425. (l) Dubois, L. H.; Caster, D. G.; Somorjai, G. A. *J. Chem. Phys.* **1980**, *72*, 5234. (m) Kesmodel, L. L.; Dubois, L. H.; Somorjai, G. A. *Ibid.* **1979**, *70*, 2180. (n) Stair, P. C.; Somorjai, G. A. *Ibid.* **1977**, *66*, 2036. (o) Lo, W. J.; Chung, Y. W.; Kesmodel, L. L.; Stair, P. C.; Somorjai, G. A. *Solid State Commun.* **1977**, *22*, 335. (p) Demuth, J. E.; Eastman, D. E. *Phys. Rev. Lett.* **1974**, *32*, 1123. (q) Skinner, P.; Howard, M. W.; Oxtun, I. A.; Kettle, S. F. A.; Powell, D. B.; Sheppard, N. *J. Chem. Soc., Faraday Trans. 2* **1981**, *77*, 1203. (r) Stuve, E. M.; Madix, R. J. *J. Phys. Chem.* **1985**, *89*, 3183; *Surf. Sci.* **1985**, *160*, 293. (s) Hills, M. M.; Parmeter, J. E.; Mullins, C. B.; Weinberg, W. H. *J. Am. Chem. Soc.* **1986**, *108*, 3554.

(44) Goodman, D. W. *Surf. Sci.* **1982**, *123*, L679.

(45) See, for example: (a) Anderson, A. B.; Hoffmann, R. *J. Chem. Phys.* **1974**, *61*, 4545. (b) Anderson, A. B. *J. Am. Chem. Soc.* **1977**, *99*, 696. (c) Howard, I. A.; Dresselhaus, G. *Surf. Sci.* **1984**, *136*, 229. (d) Rösch, N.; Rhodin, T. N. *Phys. Rev. Lett.* **1974**, *32*, 1189. (e) Anderson, A. B. *J. Chem. Phys.* **1976**, *65*, 1729. (f) Baetzold, R. C. *Langmuir*, submitted for publication.

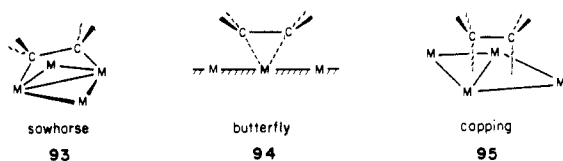
(46) (a) Dewar, M. J. S. *Bull. Soc. Chim. Fr.* **1951**, *18*, C79. (b) Chatt, J.; Duncanson, L. A. *J. Chem. Soc.* **1953**, 2939.

Table VI. Binding Characteristics of Ethylene on the Co(0001) Surface

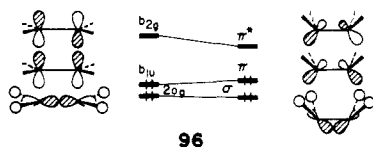
geometry	binding $E$ (eV) <sup>a</sup>	overlap population <sup>b</sup>		orbital occupation			total charge on ethylene
		C–C	C–M	$\sigma$	$\pi$	$\pi^*$	
	2.0	0.83	0.38	1.94	1.75	1.28	-1.0
	1.0	0.86	0.23	1.95	1.79	1.08	-0.4
	-0.7	0.85	0.10	1.92	1.73	0.90	-0.9

<sup>a</sup>The binding energy is defined as  $E(\text{slab}) + E(\text{planar ethylene}) - E(\text{system})$ . A positive sign means ethylene is bound. <sup>b</sup>For a comparison the C–C overlap population for the planar molecule is 1.30 and for the bent one 1.16.

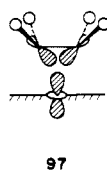
by 30° but the HCH angle remaining 120°. We are going to compare three different adsorption sites **93**, **94**, and **95**, assuming a C–M distance 2.1 Å for all. Since most experimental studies are on late transition metals,<sup>43r</sup> we will perform the calculation only for Co(0001). The choice of these geometries is based on our knowledge of organometallic compounds, in particular those in ref 38, and the structure of Zeise's salt.<sup>47</sup>



For the small degree of bending or puckering assumed, the ethylene orbitals will change little on going from the planar molecule to the puckered one. This was confirmed by calculations—**96** shows some of the valence orbitals:



$\pi$  and  $\pi^*$ , responsible for the important forward and back-donation in the Dewar–Chatt–Duncanson model,<sup>46</sup> mix in some  $\sigma$  character. Another  $\sigma$  orbital, its lobes directed inward, may also play an important bonding role, especially in geometry **95**, through an overlap of type **97**.



We compare the ethylene orbital contribution to the total DOS for those three adsorption sites, **93**, **94**, and **95** in Figure 19. Upon adsorption all occupied orbitals (up to  $\pi$ ) remain approximately where they were before adsorption. The unoccupied orbitals (above  $\pi^*$ ) are all smeared out, more so for geometry **95**.

Let us zoom in at those three orbitals  $\sigma$ ,  $\pi$ , and  $\pi^*$  whose lobes point toward the metal surface and thus should have the greatest potential for metal–ethylene interaction. The calculations (summarized in part in Table VI) show that  $\sigma$  interacts little, most in the capping geometry **95**. Even there it donates no more than 4% of its electron density to the surface. A typical interaction involved is **98**. A similar conclusion holds for  $\pi$ ; in the capping geometry  $\pi$  donates more electrons and is pushed down more. But in the butterfly geometry **94** there is no indication that the in-

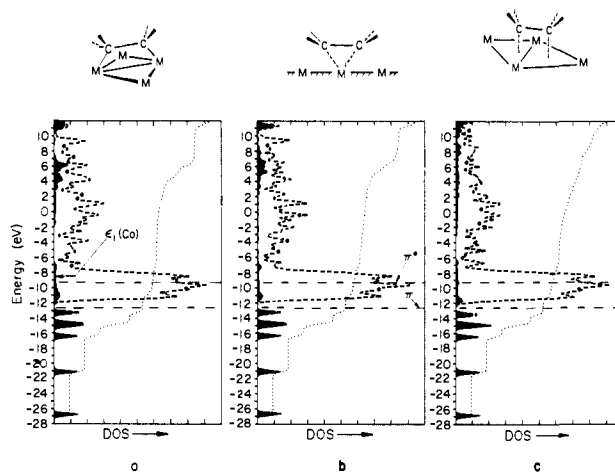


Figure 19. A comparison of total DOS for ethylene (bent) chemisorbed systems of different adsorption geometries on Co(0001): (a) the sawhorse geometry; (b) the butterfly geometry; (c) the capping geometry. The darkened area shows the ethylene contribution.

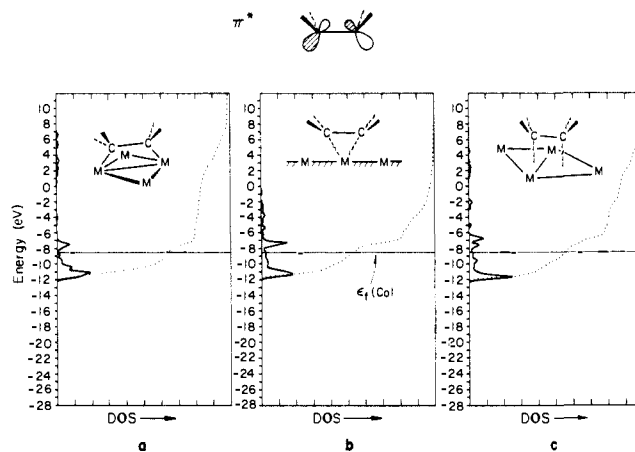
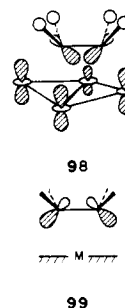


Figure 20. A comparison of ethylene  $\pi^*$  states on three adsorption geometries: (a) sawhorse; (b) butterfly; (c) capping.

teraction is stronger than in the sawhorse geometry, mostly due to the fact that  $\pi$  has its lobes pointing outward, away from the metal atom, **99**. Table VI shows that  $\pi$  has donated substantial density to the surface.



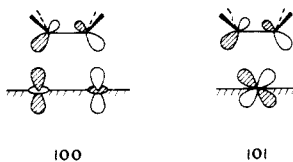
(47) Love, R. A.; Koetzle, T. F.; Williams, G. J. B.; Andrews, L. C.; Bau, R. *Inorg. Chem.* **1975**, *14*, 2653.

(48) Jorgensen, W. L.; Salem, L. *The Organic Chemist's Book of Orbitals*; Academic: New York, 1973; pp 11–17.

(49) Vannice, M. A. *J. Catal.* **1975**, *37*, 449, 462.



The biggest difference occurs in the  $\pi^*$  orbital, and for this one we offer a decomposition of the DOS in Figure 20.  $\pi^*$  is smeared out more along the energy scale as the geometry goes from **93** (sawhorse) to **94** (butterfly) to **95** (capping). In the sawhorse geometry  $\pi^*$  interacts only with the top of the d band (M-M antibonding). A characteristic interaction ( $d_{z^2}$ ) is shown in **100**. In the butterfly modes it interacts with the *entire*  $d_{xz}$  band **101**, especially those portions that match the energy of  $\pi^*$ . So we



expect the interaction to be stronger and  $\pi^*$  spread out more. The capping geometry **95** still remains the most effective for interaction and we see  $\pi^*$  dispersed most. Again this is due to the fact that more metal atoms and orbital combinations are available to interact with  $\pi^*$ . From its band width and proximity to the Fermi level we can conclude that  $\pi^*$  has the strongest interaction with the metal and is primarily responsible for the binding.

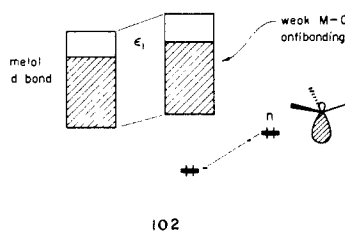
The top of the wide  $\pi^*$  band is C-M antibonding and the bottom C-M bonding. The stronger the interaction between  $\pi^*$  and metal the more profound the antibonding or bonding character. Thus at low band filling that geometry which allows stronger interaction has more bonding, but at high band filling more antibonding. This kind of reasoning can extend our considerations to surfaces other than the one considered here.

Table VI collects the bonding information for all three geometries. As we have said before, the  $\pi^*$  interaction with the metal strengthens on going from sawhorse (**93**) to butterfly (**94**) to capping (**95**) geometries. The stronger interaction for the capping geometry is supported also by the fact that ethylene donates more charge to the metal (see last column in Table VI). Our calculation also suggests that in the sawhorse geometry  $\pi^*$  is more filled and ethylene dissociation into CH<sub>2</sub>'s should be more facile.

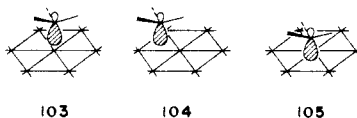
The sawhorse mode is categorized as the di- $\sigma$ -bonding and the butterfly as the  $\pi$ -bonding mode in surface science literature. Experimental studies<sup>43p</sup> as well as theoretical calculations<sup>45d</sup> tell us that  $\pi$  is pushed down more in the  $\pi$ -bonding than in the di- $\sigma$ -bonding geometry. Our calculations are no exception, but in addition they indicate the driving force behind the stronger interaction in the butterfly geometry.

## Conclusions

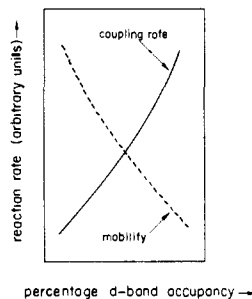
Let us summarize several important results and discuss the possible consequences. In the C<sub>1</sub> fragment part we concluded that n-CH<sub>3</sub> or  $\sigma$ -CH<sub>2</sub> (=n-CH<sub>2</sub>) is responsible for the binding of the corresponding species to the surface. n-CH<sub>3</sub> or  $\sigma$ -CH<sub>2</sub> is pushed down in energy and its bonding partner, the metal d band region, is characterized by weak M-C antibonding. This is shown schematically in **102**.



We saw what happens as the methyl group is moved from the on-top site **103** to the 2-fold bridging site **104** to the 3-fold bridging site **105**. For symmetry and overlap reasons the antibonding feature in the d-band region becomes stronger and the total energy of the system goes up along with this migration. Also the



methyl-to-metal antibonding character grows with the metal d-band filling. The binding energy decreases from most of the binding sites and at the same time the difference between the binding energies for these adsorption sites (i.e., the migration barrier) is enhanced (cf. Table II and **72**). Therefore, the methyl group becomes less mobile on the surface as the d bands are more occupied. For the same reason the binding energy of the other C<sub>1</sub> fragments to a metal surface also decreases as the metal d band is more populated (Tables IV and V). We have also found that the endothermicities and the energy barriers for the coupling of two alkyl groups or alkyl and alkylidene groups are generally lower for metals on the right side of the transition-metal series (e.g., Co). Combining this qualitative information we construct drawing **106**.



**106**

What are the consequences of **106**? First of all the fact that the CH<sub>3</sub> group (which serves as a model for longer alkyl chains) is less mobile on the surface of higher d-band filling may contribute to the experimental fact that the average hydrocarbon chain length in the FT product is *smaller* for metal catalysts at the right side of the transition series than that produced by a catalyst at the left side.<sup>50</sup> Thus, a lower mobility means a smaller probability for propagation and therefore shorter chain products. Secondly, it is experimentally known that the reactivity of an FT metal catalyst has a maximum as one moves across the transition series.<sup>49-51</sup> This extremely important experimental observation, the so-called "volcano" effect, is consistent with the opposing effects displayed in **106**. As the d band is filled, the mobility of the organic fragments (particularly that of the alkyl groups) is reduced, but at the same time their coupling requires less energy and the propagation rate increases. *A maximum in the reaction rate and the surface activity results.* Our model is, of course, very simple and naive and factors other than those discussed above may also contribute to the "volcano" effect. For example, Nørskov attributed the "volcano" effect to the decrease in binding energy on one hand and a decrease in the adsorption rate of the adsorbate on the other, along the transition series.<sup>51</sup> The decrease in binding energy, he argued, is due to an increase in the antibonding between the adsorbate and the metal. This is exactly what we have in **102**. So at the left side of the transition series the binding is so strong that it inhibits the coupling reaction and subsequent desorption. At the right side Nørskov concluded that adsorption rate is small and the reactivity low. Our study shows that the decrease in the mobility and coupling rate, factors which were not considered in his analysis, may also contribute to the low reactivity at the right side of the transition series. We have already noted earlier that the binding energies are one of the major factors that determine the thermodynamics of the coupling process. A high binding energy generally results in a highly endothermic coupling process (e.g., the propagation reaction c in Scheme III). However, we stress that the *absolute* magnitude of the binding energy of the organic radical to the metal surface is not the *only* important

(50) (a) Bond, G. C. *Catalysis by Metals*; Academic: New York, 1962. (b) Boudart, M. *Kinetics of Chemical Processes*; Prentice-Hall: Englewood Cliffs, NJ, 1968. (c) See also Chapter 4 in ref 1e; Sinfelt, J. H. in ref 1f, Vol. 1, Chapter 5; Schwab, G.-M. in ref 1f, Vol. 2, Chapter 1.

(51) (a) Nørskov, J. K. *Physica* **1984**, *127B*, 193. (b) Holloway, S.; Lundqvist, B. I.; Nørskov, J. K. *Proceedings of the 8th International Congress on Catalysis*; Verlag Chemie: Weinheim, 1985; 4, IV85-IV95.

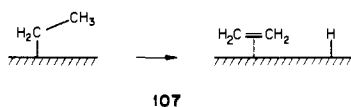
Table VII. Extended Hückel Parameters

	orbital	$H_{ii}$ , eV	$\zeta_1^d$	$\zeta_2$	$c_1^a$	$c_2$
Co	3d	-9.7	5.55	1.9	0.5448	0.6556
	4s	-7.8	2.0			
	4p	-3.8	2.0			
Cr	3d	-7.9	4.95	4.6	0.4876	0.7205
	4s	-7.3	1.7			
	4p	-3.6	1.7			
Ti	3d	-5.9	4.55	1.4	0.4206	0.7839
	4s	-6.3	1.5			
	4p	-3.2	1.5			
C	2s	-21.4	1.625			
	2p	-11.4	1.625			
H	1s	-13.6	1.3			

<sup>a</sup> Exponents and coefficients in a double- $\zeta$  expansion of the 3d orbital.

factor. The *relative* binding energies, which determine the surface mobilities of these fragments, are also important. Furthermore, absolute and relative binding energies are not necessarily related. Thus, a strongly bound fragment is not necessarily "unreactive", provided that it migrates easily from one metal site to the other (e.g., the binding energy of CH<sub>3</sub> on Ti is 1.7 eV higher than that on Co, but the migration barrier on Ti is lower than that on Co) and that the barrier for its coupling is low.

We note that many other factors that may play an important role in the FT synthesis were not considered in our study. One is the relation between the metal's d occupancy and the rate of the dissociative chemisorption of the reactants, such as CO.<sup>19a</sup> A second is the dependence of the rate of the reductive-elimination reaction 107 on the metal's d occupancy.



At this point we conclude our first glance at the FT reaction. So much more remains to be done, and with better calculations than ours. But we believe that we have gained some insight into the essence of the bonding of CH<sub>3</sub>, CH<sub>2</sub>, CH, and C<sub>2</sub>H<sub>4</sub> to metal surfaces, and the migration propensity and coupling capabilities of these important surface species. One useful conceptual decomposition of the barriers, often small, sometimes large, that are found on the way to products, is the following: there are preferred sites of chemisorption, differential barriers to migration on the

surface, a "proximity" or crowding effect for the assembly of fragments prior to reaction, and, finally, an activation energy for actual coupling and desorption.

**Acknowledgment.** This research was supported by the Office of Naval Research and by the National Science Foundation through Grant CHE 84-06119 and Grant DMR 821722 to the Material Science Center at Cornell University. We are grateful to Anne Turner for the typing, to Linda C. Kapitany for corrections and assembly, and to Jane Jorgensen and Elisabeth Fields for the drawings.

#### Appendix I

All calculations are of the extended Hückel tight binding type,<sup>14</sup> with the parameters given in Table VII. The M-C distance is chosen to be a fixed 2.1 Å throughout the calculations although experimental data indicate different M-C distances for various adsorption sites and different C<sub>1</sub> fragments.<sup>22</sup> The choice of a constant M-C distance comes from our experience that overlap populations for bonds of "unbiased" or equal length will be indicators of the relative bond strengths. The Co-Co distance in the hcp slab is 2.51 Å,<sup>20a</sup> C-H = 1.09 Å. The total energies, DOS and COOP, are calculated on a 10-k-point set from ref 53, but wherever symmetry permits the 10-k-point set is reduced to a 7 or 5 special k point set.

#### Appendix II

The choice of the metal slab thickness was based on previous exploratory calculations on up to 5 layers.<sup>15,19a,21</sup> A 3-layer slab was found to be a good compromise between accuracy and economy. To ensure the above conclusion, we have performed calculations for CH<sub>3</sub> on a 7-layer Co slab in "on-top", the "bridging", and the "capping" geometries. The binding energies (cf.  $E_1$  in Table III) are 3.51, 2.24, and 1.74 eV, respectively, not much different from those for the 3-layer slab. The total charges on CH<sub>3</sub> are -0.59, -0.55, and -0.52. Other properties derived from the 7-layer slab also hold the same trends calculated for a 3-layer slab.

**Registry No.** CH<sub>3</sub>, 2229-07-4; CH<sub>2</sub>, 2465-56-7; CH, 3315-37-5; Ti, 7440-32-6; Cr, 7440-47-3; Co, 7440-48-4.

(52) Sinfelt, J. H. in ref 1f, Vol. 1, p 282. Sinfelt, J. H. *J. Catal.* **1973**, *29*, 308. Sinfelt, J. H. *Acc. Chem. Res.* **1977**, *10*, 15. *Sci. Am.* **1985**, *253*, No. 3, 90.

(53) Pack, J. D.; Monkhorst, H. J. *Phys. Rev. B* **1977**, *16*, 1748.